Always-on wireless ear-EEG to monitor brain activity: Electronics design

Author
Cyril Arnold Weustink

TU Delft

Always-on wireless ear-EEG to monitor brain activity: Electronics design

by

C.A. Weustink

Student number: 4692586
Project duration: 16 November 2021 – 30 August 2022

TU Delft

Abstract

Currently, EEG recordings are mostly made using scalp recording devices. These devices are typically difficult to put on and bulky, limiting their use to a lab environment. In-ear EEG recording is proposed as a more practical alternative to scalp EEG recording. In-ear EEG replaces the scalp electrode array with more discrete earpieces, recording the EEG signals from the ear canal instead of the scalp. Because of their increased convenience with respect to their scalp electrode array counterpart, the earpieces allow for everyday use, enabling the possibility of long-term EEG recording, outside of a lab environment.

This work presents the design of a fully-integrated in-ear EEG device. The device has been designed to record EEG signals, process them locally, and transmit the processed data to a smartphone or personal computer. The device is made to be easily re-programmable, making it possible to change the device firmware depending on the intended application. This functionality has been integrated into a small form factor, to allow for the integration of the electronics into an earpiece. A low-power design has been created, to allow for long-term battery operation.

Two prototypes have been made. The first prototype focuses on exploring different system configurations, with the small form factor less of a priority. The performance of the prototype is tested by comparing it to a commercially available scalp EEG recording device based on scalp EEG recordings. For this comparison, the auditory steady-state response (ASSR), steady-state visual evoked potential (SSVEP), and alpha-band modulation paradigms are used. The prototype has shown similar performance to the scalp EEG device in these experiments, with the scalp EEG device performing slightly better for the ASSR and alpha-band modulation paradigms, while the prototype showed the best performance for the SSVEP paradigm.

The second prototype realises the best-performing system configuration that has been found with the first prototype into a form factor that fits into an earpiece. Ear EEG experiments are performed, with electrodes placed around the ears. The ASSR, SSVEP, and alpha-band modulation paradigms have again been used in these experiments. The measured performance on the ASSR and alpha-band modulation paradigms are slightly worse than that measured using the scalp EEG experiments. The SSVEP experiments showed significantly worse performance compared to the scalp EEG experiments. These results align with the expectations, as ear EEG has been documented to have performance close to scalp EEG for the ASSR and alpha-band modulation paradigms, while the SSVEP performance is typically worse for ear EEG than for scalp EEG.

Preface

This thesis is written in order to obtain the degree of master of science in electrical engineering at the Delft University of Technology. The subject of this thesis, "Always-on wireless ear-EEG to monitor brain activity", has been conceived by dr. Dante Muratore, my supervisor during this project.

I would like to express my gratitude to dr. Dante Muratore for introducing me to this interesting project, as well as for his guidance and support. I would also like to thank my fellow students for their useful feedback and insights during the biweekly group meetings. In particular, I would like to thank Patricija Burgar and Michael Treffers, with whom I have had the pleasure of working during the project.

Lastly, I wish to thank my girlfriend, friends, and family for their enthusiasm and support, keeping me motivated throughout the project.

C.A. Weustink
The Hague, July 2022

Contents

1

Introduction

Electroencephalography (EEG) is a non-invasive method of measuring voltage variations that result from the activity of neurons in the brain. Typically these measurements are performed using electrodes placed on the scalp of a subject. Figure 1.1 shows a typical scalp EEG setup.

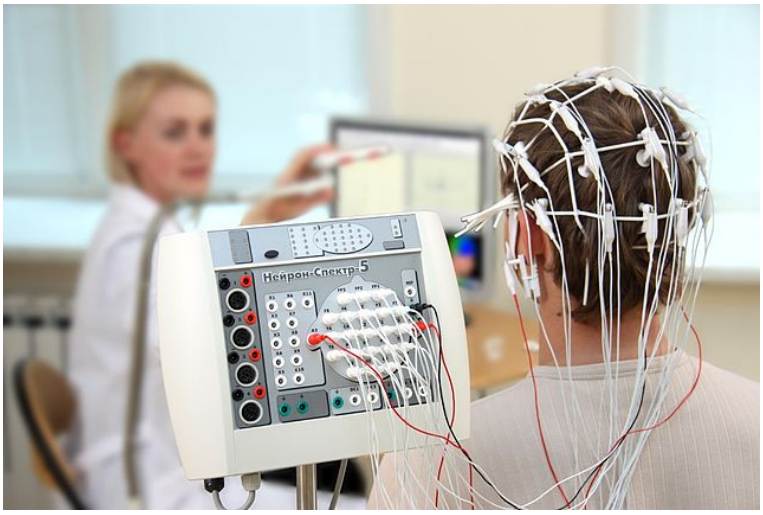

Figure 1.1: A typical scalp EEG recording setup. Source: Adapted from [1]

EEG is used as a diagnostic tool for many different brain-related disorders, like epilepsy, dementia, and sleep disorders. The use of EEG in studying these disorders is valuable, but the bulky nature of a traditional scalp-EEG measurement setup means that its use is mostly limited to short-term experiments in a clinical environment. The creation of a portable EEG device, that can be used throughout the day, would enable the use of EEG for new applications:

- Long-term measurements, which can be useful for monitoring brain disorders for which the symptoms are not visible at all times, like epilepsy
- Closed-loop nerve stimulation, activating the stimulation based on the EEG recording
- Brain-computer interfaces

In-ear EEG is proposed as a way to achieve this portability, replacing the bulky scalp electrodes with a more convenient and discrete earpiece, with the recording electrodes placed inside the ear canal.

Recently, the concept of in-ear EEG has been explored in several publications. In most of these publications, the in-ear electrodes are compared to scalp electrodes. This is typically done using the same recording electronics used for the scalp EEG measurements, which are not suitable for portable measurements. Only a few

publications are available where the in-ear electrodes are combined with portable recording electronics, actually resulting in a portable EEG device [2]–[4]. These designs explore wireless connectivity, onboard signal processing, programmable hardware, and integration of the electronics into an earpiece, but none of them combines all these features into a single device.

This project aims to design a complete in-ear EEG system, combining the electrodes and electronics into a single earpiece. The system is meant as a tool to explore the possible uses of in-ear EEG. Because of this, it will be made programmable, making it possible to change the firmware based on the intended application. The system should be able to process the recorded data on-board and communicate wirelessly to other devices. The combination of a completely wireless, portable design, on-board processing capabilities, and the ability to re-program the device depending on its application sets it apart from currently existing implementations of in-ear EEG devices.

The project consists of three parts:

- Design of dry electrodes to be placed in the earpiece
- Design of the electronics system
- Creation of the data processing algorithms

The design of the dry electrodes is done by Patricija Burgar [5] and the data processing algorithms are created by Michael Treffers [6]. This thesis describes the design process of the electronics system.

In Chapter 2, the principles behind EEG, and the specifics of in-ear EEG are explored. Existing portable EEG devices are also examined and compared. Based on these findings, a prototype of an in-ear EEG recording device is designed. The design process of this prototype is described in Chapter 3. The prototype is then tested and compared to a scalp EEG recording device in Chapter 4. A second, more compact prototype is then designed and tested, based on the findings from the first prototype. This process is described in Chapter 5. In Chapter 6, the performance of the final prototype is evaluated based on EEG recordings from around the ears. The thesis is concluded with a discussion of the results and suggestions for future work in Chapter 7.

2

Background knowledge and state of the art

2.1. Characterization of EEG signals

Typically, EEG signals have an amplitude ranging between 2 μV_{pp} and 100 μV_{pp} [7]. They can be divided into five different types of brain waves [8]:

- **Delta -** Delta waves are the lowest frequency brain wave, with frequencies ranging between 0.5 and 4 Hz. This type of brain wave is present when the subject is asleep.
- **Theta -** Theta waves have frequencies ranging between 4 and 8 Hz. They are present when the subject is deeply relaxed or inward-focused.
- **Alpha -** Alpha waves have frequencies ranging between 8 and 12 Hz. They are present when an individual is very relaxed and has passive attention.
- **Beta -** Beta waves have frequencies ranging between 12 and 35 Hz. They occur when someone is active, with external attention. When someone has anxiety, Beta waves are also present.
- **Gamma -** Gamma waves are the highest frequency brain wave with frequencies above 35 Hz. These occur when the subject is concentrating.

Detection of a specific type of brain wave can be used to get an indication of the mental state of the subject. For instance, when delta waves are dominant in the EEG measurements, this is an indication that the subject is asleep. For this purpose, frequency domain analysis is often used.

Artefacts in the recording can reduce the system signal-to-noise ratio. Examples of these artefacts are blinking, eye movement, or muscular activity recorded on top of the EEG signals. Movement of the applied electrodes could also cause artefacts to occur [8]. Interference caused by the coupling to the power lines is also often present in EEG measurements.

2.2. Recording hardware

EEG devices typically consist of several recording channels. The structure of a single EEG recording channel is shown in Figure 2.1. Each part of the recording channel has its own set of requirements.

2.2.1. Electrodes

Electrodes used in EEG applications can be divided into two main categories: wet and dry electrodes. Wet electrodes use a gel to improve the contact between the electrode and the skin, resulting in low electrode-skin impedance (ESI). Dry electrodes do not use gel and rely on physical contact between the electrode and the skin, resulting in a higher impedance seen at the skin-electrode interface [2]. Low ESI is generally desired to reduce the signal noise caused by the electrode. Wet electrodes therefore typically provide the best performance. Dry electrodes are mostly used for their convenience, not requiring the application of a gel. To improve the performance of dry electrodes, pressure can be applied to electrodes. Doing so ensures that proper mechanical contact is achieved between the electrode and skin [2].

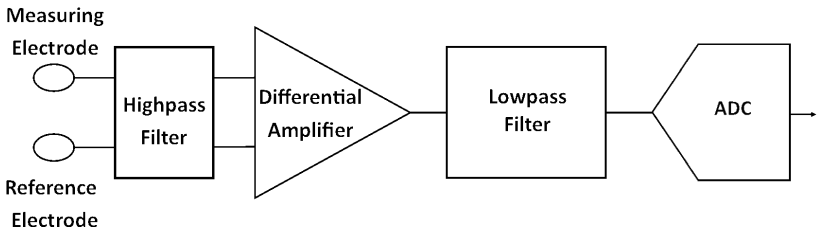

Figure 2.1: Structure of an EEG recording channel.

EEG signals are typically measured using two electrodes, one electrode acting as the measuring electrode and the second acting as a reference. In most cases, a third electrode is included, used to reduce the common-mode signal seen at the electrodes by providing common-mode feedback. This electrode is often called the ground electrode.

2.2.2. Amplifier

The amplifier must adhere to a set of requirements to ensure the signal is not distorted.

- **Input impedance -** For wet electrodes, the impedance seen at the skin-electrode interface is usually below 5 kΩ in the frequency range of interest (0.5 Hz - 100 Hz) [9]. For dry electrodes, the impedance is typically one order of magnitude higher [10]. The input impedance of the amplifier is required to be significantly higher than this, to prevent a large voltage drop across the electrode-skin interface. Additionally, when the measuring and reference electrode impedances are not equal, part of the common-mode signal that is seen by the electrodes can be turned into a differential signal. This signal will be amplified by the differential amplifier, which can cause distortion of the recording. The higher the input impedance of the amplifier, the smaller this effect is [11]. A spreadsheet has been made to analyse the input impedance requirements for different common-mode voltages and impedance offsets [12].
- **Common-mode rejection ratio -** The amplitude of EEG signals tends to be several orders of magnitude smaller than the common-mode signal seen at the electrodes. It is important that the common-mode signal is not amplified, as this would likely result in the differential signal being drowned out. A high common-mode rejection ratio (CMRR) is required to ensure this does not happen. In modern EEG systems this CMRR is at least 80 dB and typically around 100 dB [13].
- **DC-offset -** As a result of differences in the electrode-skin interface between electrodes, a DC offset voltage can be present. When using an ordinary differential amplifier, this offset is amplified and will saturate the amplifier. Measures need to be taken to deal with this offset voltage. A high-pass filter can be used before the amplifier to remove the DC offset, avoiding saturation of the amplifier. Alternatively, a high dynamic range amplifier can be used that can record the DC offset, as well as the EEG signals.
- **Input referred noise -** The input referred noise of the amplifier must be below $2\,\mu V_{pp}$, typically the minimum magnitude of EEG signals.

Many different design approaches have been proposed to adhere to these requirements [14]. To meet the input impedance requirement, op-amps are often used as a buffer stage, as op-amps characteristically have a very large input impedance. Clever topologies can be used to increase the CMRR of amplifiers, like is done in the well-known three op-amp instrumentation amplifier topology. Additionally, the subject can be biased using a bias amplifier, reducing the magnitude of the common-mode signal seen at the electrodes.

2.2.3. Filters

In case of EEG recording, only low frequencies (<100 Hz) are of interest [13]. Any signal recorded above this frequency can be filtered out, preventing aliasing of the signal into the band of interest during sampling. A low-pass filter can be introduced to remove these higher frequencies. A high-pass filter is often used to filter out any DC signals before they enter the amplifier. This is done to avoid saturation of the amplifier. This concept is visualized in Figure 2.2.

Often an extra filter is added to remove the power line interference. A notch filter is used to achieve this

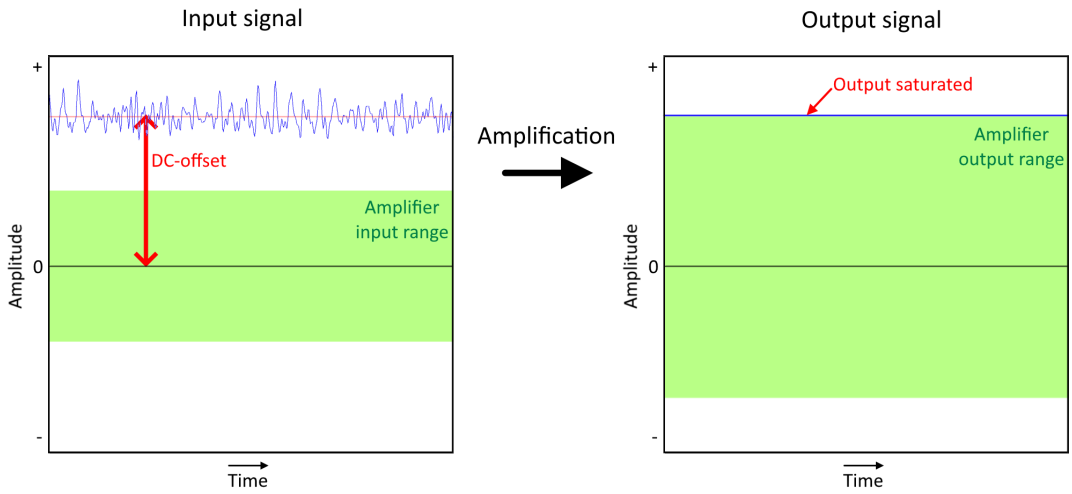

(a) Amplification without a high-pass filter at the input of the amplifier.

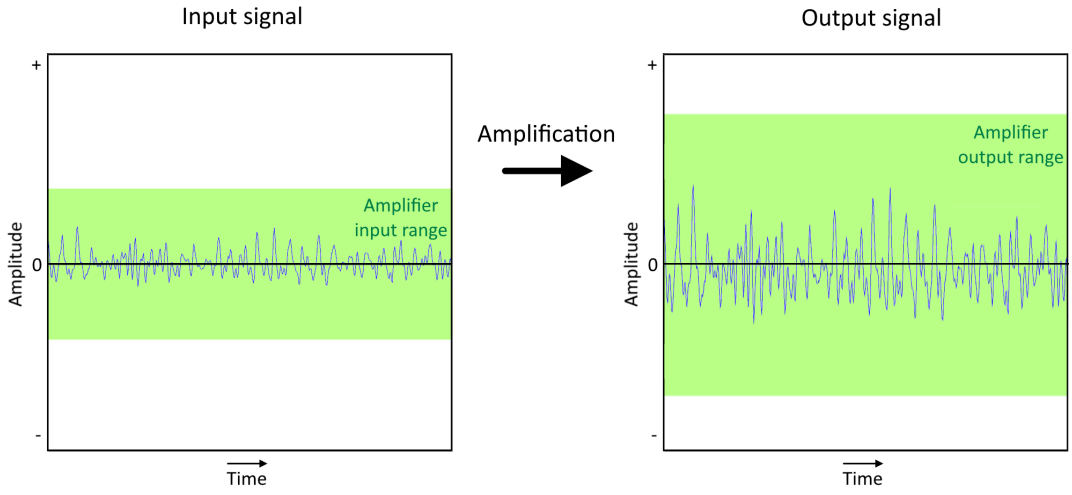

(b) Amplification with a high-pass filter at the input of the amplifier.

Figure 2.2: Amplification without the removal of the DC offset using a high-pass filter (a), and with the removal of the DC offset using a high-pass filter (b).

[15]. The application of a notch filter can distort the amplitude and phase of the signal. Because of this, a notch filter is only used if other measures of removing the power line interference, like shielding of the device, are not sufficiently effective [13]. Power line interference can also be removed by means of a digital filter, removing the need for additional components.

2.2.4. Analog-to-digital converter

To get an accurate digital representation of the recorded EEG signals, the analog-to-digital converter (ADC) must adhere to a set of requirements.

- **Low power -** For portable EEG devices, low power consumption is desired to allow for battery-powered operation. A low-power ADC is therefore desired.
- **Low frequency -** Because EEG signals are of relatively low frequency, the implemented ADC does not have to be capable of very high sampling frequencies. An ADC that operates efficiently at low sampling frequencies is therefore preferred. A sampling frequency of at least 200 Hz is required to cover the entire frequency range between 0.5 Hz and 100 Hz.
- **Resolution -** The ADC must have a resolution of at least 8 bits to achieve the minimum dynamic range of 2 μV_{pp} - 100 μV_{pp} to record EEG signals. If the DC offset and power line interference are not removed before the input of the ADC, the resolution should be higher, as the upper limit of the dynamic range should then be high enough to include the interfering signals, while the lower limit does not change.

A popular type of ADC used for the processing of low-frequency biosignals is the successive approximation register (SAR) ADC. The SAR ADC is popular for use with biosignals, because the power consumption scales with the sample rate that is used, as it usually has no static dissipation [16]. When operating at the low frequencies required for EEG recording, this allows for very low energy consumption.

Another popular ADC type is the Sigma-Delta ADC. Sigma-Delta ADCs are capable of noise shaping: most of the quantization noise is present at the highest signal frequencies [17]. This is useful when recording low-frequency biosignals. As a result of the low quantisation noise at low frequencies, the dynamic range of a Sigma-Delta ADC can be higher than that of a SAR ADC for low-frequency signals.

2.3. Wireless communication

In wireless EEG systems, two different approaches are common. The first approach is to transmit the complete recorded data stream, as is done by Dias et al. [18]. A second option is to process the recorded data on the recording device, before transmitting the processed data. This approach is used by Kaveh et al. [2]. Doing this can reduce the amount of data that needs to be transmitted, which in turn reduces the transmission power consumption. Provided the size of the data stream is reduced significantly, processing on the device can actually be more power efficient than transmitting the entire data stream.

For portable EEG applications, low power consumption is desired. The most prominent protocols used for low-power, wireless communication in health monitoring systems are Bluetooth Low Energy (BLE) and Zigbee [19].

Bluetooth Low Energy is a wireless communication protocol aimed at short-range, low-power applications. It has a range of 10 m, making it suitable as a link for communication to a base station in the same room. BLE operates at 2400 MHz and offers a bit rate of 1 Mb/s. As the name suggests, BLE is a low-energy protocol, with power consumption ranging between 10 µW when sustaining a connection without transmitting data and 10 mW at the maximum data transmission rate. This makes it suitable for battery-powered devices.

The Zigbee protocol is aimed at low-power, medium-range applications. With a range of 100 m, wireless communication throughout an entire house is made possible. Zigbee can operate at different frequencies and bit rates. When operating at 868 MHz, a bit rate of 20 KB/s is achieved. At 915 MHz, the bit rate is 40 KB/s. The maximum bit rate of 250 KB/S is achieved at 2400 MHz. The transmission power for Zigbee ranges between 0.6 µW when sustaining a connection without transmitting data and 1 mW at the maximum data transmission rate.

Table 2.1: Comparison between Bluetooth Low Energy and Zigbee.

	Range	**Max. bit rate**	**Min. transmission power**	**Max. transmission power**
Bluetooth Low Energy	10 m	1 Mbit s^{-1}	10 µW	10 mW
Zigbee	100 m	250 kbit s^{-1}	0.6 µW	1 mW

When comparing Bluetooth Low Energy and Zigbee, as is done in Table 2.1, both technologies are comparable when it comes to power consumption. BLE is most suitable when a high bit rate is required and only a short range is needed. Zigbee is more suitable when a higher range is required. Bluetooth Low Energy is compatible with many devices, as most modern smartphones and personal computers are BLE compatible. This is not the case for Zigbee, which often requires additional hardware.

2.4. Characteristics of in-ear EEG

Recording of EEG signals from the ear, instead of from the scalp, poses several benefits, but also new challenges. A clear benefit of in-ear EEG is its portability. The application of an earpiece is less bothersome than the application of a full electrode array on the scalp, regardless of whether wet- or dry electrodes are used. This promotes use outside of a lab environment. Portability of in-ear EEG devices is therefore desired, which has an effect on the electronics that can be used. The electronics are preferably small and should have low power consumption.

Because the placement of the recording electrodes is limited to the inside of the ear, it is not possible to gather information from all areas of the brain. When using the same reference electrode, located at the top of the scalp, the signals that can be recorded by means of in-ear measurement are almost identical to the signals recorded by electrodes placed near the ear by means of scalp measurement [20]. Scalp referencing is not very practical for in-ear EEG measurement. Because of this, another way of referencing is needed. Mikkelsen et al. propose to use an electrode placed on the concha of the ear as a reference [20]. This location, shown in Figure 2.3, is chosen because of its large distance from the ear canal. With a small distance between the measuring and reference electrodes, the signals seen at both electrodes are likely to be similar. This will result in a cancellation of the signal when differential amplification takes place. For this reason, a large distance between the measuring and reference electrodes is desired.

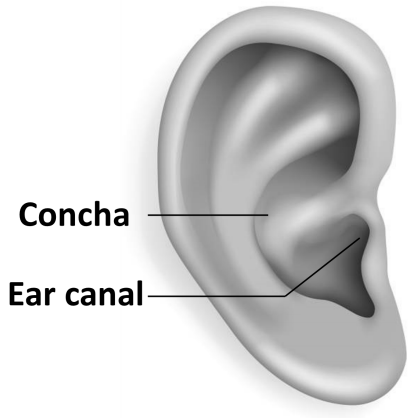

Figure 2.3: Possible location for a reference electrode on the concha of the ear.

Another referencing method, proposed by Mikkelsen et al., is to reference the electrodes in one ear to electrodes placed in the other ear [20]. This method of referencing assumes a setup consisting of two earpieces.

2.5. Performance of in-ear EEG

2.5.1. Commonly used EEG paradigms

EEG paradigms can be used to assess the performance of an EEG device. These paradigms involve stimulation of the subject, evoking a response in the neural activity. Some commonly used paradigms are listed.

Auditory steady-state response (ASSR)
In the auditory steady-state response paradigm, an auditory stimulus is presented to the subject. This stimulus, often a white noise signal, is amplitude modulated at a known frequency [20], [21]. The modulation frequency of the signal becomes visible when performing an EEG recording. Typically a modulation frequency of 40 Hz is chosen, as the effect is most prominent at this frequency [22]. By averaging the power spectrum of the measured EEG signal over time, a peak should become visible in the spectrum at the modulated frequency. The amplitude of this peak with respect to the neighbouring frequencies can be used as a comparative measure of performance.

Steady-state visual evoked potential (SSVEP)
The steady-state visual evoked potential is similar to the ASSR, but instead of an auditory stimulus, a visual stimulus is used. By modulating a light source with a specific frequency, neural activity is evoked at that same frequency. This again becomes visible in EEG recordings. Harmonics of the stimulation frequency are also detectable [21].

Alpha-band modulation
The alpha band modulation paradigm relies on the difference in presence of alpha waves when the subject is in a state of concentration or in a state of relaxation. As mentioned in Section 2.1, alpha waves are present when someone is in a relaxed state. By performing EEG measurements on a subject in a concentrating state, for instance when performing a calculation, and in a relaxed state, a difference can be detected in the recorded signal power in the alpha band (8-12 Hz) [20].

2.5.2. ASSR performance

Mikkelsen et al. have compared the ASSR performance of an in-ear earpiece using wet electrodes to wet scalp electrodes [20]. The scalp electrodes are placed at the TP_7 ,TP_8, TP_9 and TP_{10} locations, following the modified combinatorial nomenclature system shown in Figure 2.4 [23]. They have found that, when it comes to ASSR, the in-ear electrodes can obtain similar performance to on-scalp electrodes placed near the ear, finding an average SNR of 22.1±8.1 dB, while for the scalp electrodes the measured SNR was 21.8±4.0 dB. Here the SNR is defined as the difference between the logarithm of the power at 40 Hz (signal frequency) and the logarithm of the average power in the neighbouring 5 Hz intervals. The in-ear electrodes are referenced to an electrode placed at the concha of the same ear, while the scalp electrodes are referenced using an electrode placed at the top of the scalp at the C_Z location. An interesting finding is that there is a significant difference in the SNR achieved in the ASSR measurements between the ears, likely caused by the differences in brain activity between the brain halves.

Similar results have been found in studies conducted by Kidmose et al., with the SNR achieved by the in-ear configuration even surpassing the SNR of the on-scalp configuration by 11.1 dB on average [24].

Kappel et al. [21] have performed a similar experiment, but instead of using wet electrodes for the earpieces, dry earpieces are used. The testing setup is identical to that used by Mikkelsen et al.. The SNR achieved using dry electrodes was on average 14 dB for both the left and right ear, while the average SNR achieved using the wet scalp electrodes was 17 dB for the electrode at TP_7 and 18 dB for the electrode placed at TP_8.

Although the SNR achieved using the dry in-ear electrodes is significantly smaller than that achieved by the wet scalp electrodes, the SNR is still sufficient for statistically significant observation of the ASSR. Interestingly, when referencing the dry in-ear electrodes using the wet scalp electrode placed at the Cz location, an SNR of 20 dB was achieved for the left ear and of 22 dB for the right ear. This is higher than the SNR achieved using the wet scalp electrodes. In studies conducted by Kaveh et al. and Goverdovsky et al. similar results are found, with the SNR achieved by the dry in-ear electrodes smaller than that of the wet on-scalp electrodes, but still statistically significant [25], [2]. Table 2.2 shows an overview of the in-ear ASSR SNR found by different studies. It should be noted that the studies conducted by Goverdovsky et al. and Kaveh et al. both use a user generic earpiece, while Kappel et al. use a custom-fit earpiece. This could be the reason for the slightly higher SNR found by Kappel et al..

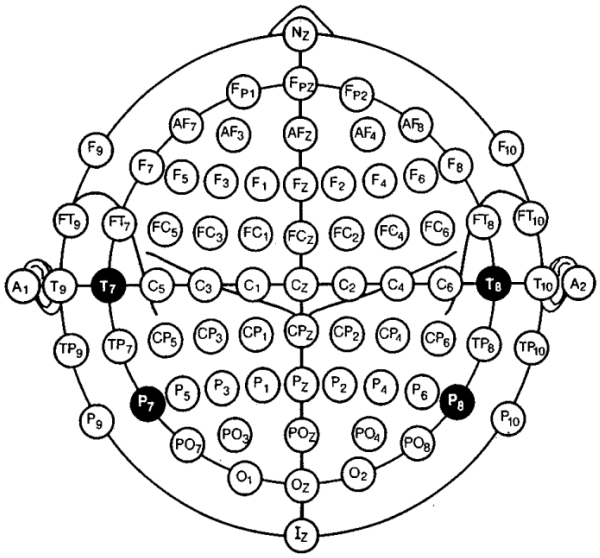

Figure 2.4: The modified combinatorial nomenclature system.
Source: Adapted from [23]

Table 2.2: The ASSR performance found for different in-ear EEG devices.

Paper	**Electrode type**	**Ear-fit**	**Average SNR**
Mikkelsen et al. [20]	Wet	Custom-fit	21.1 dB
Kidmose et al. [24]	Wet	Custom-fit	35.0 dB
Kappel et al. [21]	Dry	Custom-fit	14 dB
Kaveh et al. [2]	Dry	Generic	5.94 dB
Goverdovsky et al. [25]	Dry	Generic	10 dB

2.5.3. SSVEP performance

Using the same device setup as used for the ASSR experiment, Kappel et al. also compared the SSVEP performance of a dry in-ear EEG device to a setup using wet scalp electrodes [21]. The electrode placement is identical to the placement used for the ASSR measurements, as explained in Section 2.5.2. The modulation frequency used in the experiment is 9 Hz. The SNR achieved by the dry in-ear earpieces is 11 dB for the left ear and 12 dB for the right ear. This is the SNR of the first harmonic, located at 9 Hz in the power spectrum. The average SNR achieved for the first harmonic by the wet scalp electrodes is 22 dB for the electrode located at the TP_7 location and 23 dB for the electrode placed at the TP_8 location.

When referencing the in-ear electrodes to the electrode placed at the C_Z location, similar performance is achieved to the on-scalp electrodes, with an SNR achieved of 23 dB for the left ear and 22 dB for the right ear.

Kidmose et al. have performed a similar study, only using a custom-fit wet earpiece instead [24]. In their studies, an average SNR of 10 dB has been achieved with the custom-fit wet earpiece. Interestingly this is lower than the SNR found by Kappel et al., while better performance is expected when using wet electrodes.

2.5.4. Alpha-band modulation performance

To assess the alpha-band modulation performance of their in-ear EEG device, Mikkelsen et al. have used a test setup where someone is asked to repeatedly do some simple arithmetic in their head and subsequently rest with their eyes closed. This has been done in an altering fashion in segments of 60 seconds each. The increase in alpha waves during the resting phase of the experiment was clearly visible for the wet in-ear elec-

trode setup, referenced to an electrode placed at the concha of the same ear. The results are comparable to those found when using a wet scalp electrode setup, the scalp electrodes providing slightly better contrast between the focused and resting states.

The same experiment has been performed by Kappel et al. [21], only using dry in-ear electrodes instead of wet electrodes. They found that the alpha waves are also visible for the dry in-ear electrodes, albeit not as clearly as for the wet in-ear electrodes. The same results have been found by Kaveh et al. [2] in a similar experiment.

2.6. Existing portable EEG implementations

2.6.1. Kaveh et al. [2]

Kaveh et al. have designed a wireless in-ear EEG recording device, using a user-generic earpiece with dry electrodes. The device incorporates a wireless neural recording module called the WANDmini, which is a miniaturized version of the WAND module designed by Zhou et al. [26]. The WANDmini contains a low-energy Bluetooth antenna for wireless transmission of recorded data to the receiver antenna. An SoC FPGA is included to enable onboard signal processing, although this functionality is not yet used in the designed device. The FPGA passes on the digitized recording signals to the Bluetooth antenna.

For extraction, amplification, and digitization of the EEG signals, the NMIC integrated circuit, designed by Johnson et al., is incorporated in the WANDmini [27]. The NMIC is capable of recording and stimulating 64 EEG channels simultaneously and digitization of the input signal with a 15-bit resolution. The total power dissipation of the WANDmini is equal to 46 mW. This is low enough to allow for battery operation. An overview of the specifications of the WANDmini with NMIC is shown in Table 2.3. Figure 2.5 shows the system architecture of the WANDmini.

Table 2.3: Specifications of the WANDmini

WANDmini	
Number of channels	64
Input range	100 mV_{pp}
Input-referred Noise	71 $nV/\sqrt{Hz}$
ADC resolution	15 bits
ADC sample rate	1 kS/s
Power dissipation	46 mW

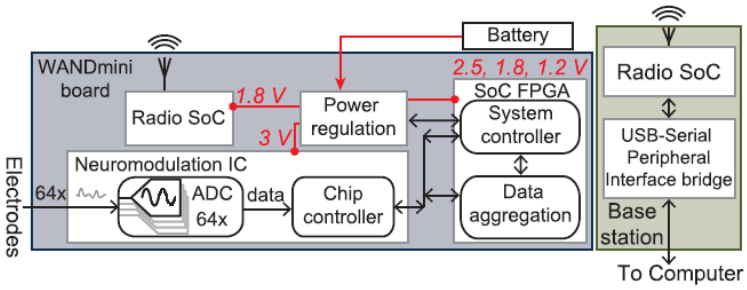

Figure 2.5: The system architecture of the WANDmini.
Source: Adapted from [2]

2.6.2. Sintotskiy and Hinrichs [3]

The portable in-ear EEG device designed by Sintotskiy and Hinrichs uses universal earpieces with wet electrodes. Instead of using wireless transmission of the recorded data, a USB interface is used, which enables connection to a smartphone. The recording electronics are based around the ADS1299, produced by Texas Instruments [28]. The ADS1299 combines amplification and digitization functionality and has a bias amplifier for the reduction of the common-mode signal. The digitised signal is communicated to a microcontroller using a Serial Peripheral Interface (SPI) bus. The microcontroller that is used is an Arduino Nano V3.0. The microcontroller supplies the ADS1299 with power. The digitised signal, communicated via the SPI, is pre-

sented on the USB bus of the Arduino, which can then be connected to a smartphone to read out the signals. A sampling rate of 250 Hz is used. This sampling rate is chosen because it is sufficiently high to record the frequency band of interest with only a small data stream, which is good for power efficiency. A complete overview of the specifications of the device is shown in Table 2.4. An image of the device is shown in Figure 2.6.

Table 2.4: Specifications of the portable EEG device designed by Sintotskiy and Hinrichs

In-ear EEG for home monitoring	
Number of channels	2
Input range	± 562.5 mV
Input-referred Noise	≤ 1 μV_{pp} (70 Hz BW)
Common-mode rejection	≥ 110 dB (at 50/60 Hz)
ADC resolution	24 bits
ADC sample rate	250 Hz
Power dissipation	max. 595 mW

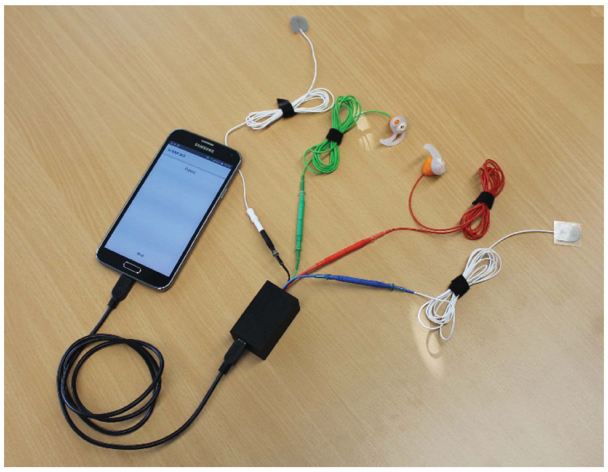

Figure 2.6: The portable EEG device developed by Sintotskiy and Hinrichs.
Source: Adapted from [3]

2.6.3. Lee et al. [4]

With all electronics integrated into the earpiece, Lee et al. have created a truly portable wireless ear-EEG device. The device is capable of recording EEG over 2 channels and also incorporates a speaker to generate tones to be used in auditory steady-state response applications. Amplification of the EEG signals is performed using a two-channel instrumentation amplifier. This amplifier uses capacitive coupling to account for any DC offset between the electrodes. Common-mode feedback is used to reduce the common-mode voltage seen at the amplifier inputs. Digitisation of the analog signal is done by means of an 11-bit SAR ADC.

The digitised signal is transmitted using a body channel communication transceiver, which uses the user's body as the transmission medium, allowing for low power transmission. To reduce the power dissipation of the electronics, a sleep mode is introduced. When the sleep mode is active, no EEG recordings are made and the audio analog front end and body channel communication transceiver are deactivated to reduce the power dissipation. By using this approach it becomes possible to operate the device using a very small battery, which can be incorporated into the earpiece. The total peak power consumption in active mode is equal to 12.3 mW. In sleep mode, the total power consumption is only 31 µW. A complete overview of the device specifications is shown in Table 2.5. A block diagram of the designed integrated circuit is shown in Figure 2.7.

Table 2.5: Specifications of the In-Ear BCI Controller IC With EEG Instrumentation Amplifier by Lee et al.

In-Ear BCI conroller	
Number of channels	2
Input-referred Noise	$\leq 0.38\,\mu V_{rms}$ (0.5 - 100 Hz)
Common-mode rejection	≥ 95 dB
ADC resolution	11 bits
ADC sample rate	2 kHz
Power dissipation (active mode)	max. 12.3 mW
Power dissipation (sleep mode)	avg. 31 µW

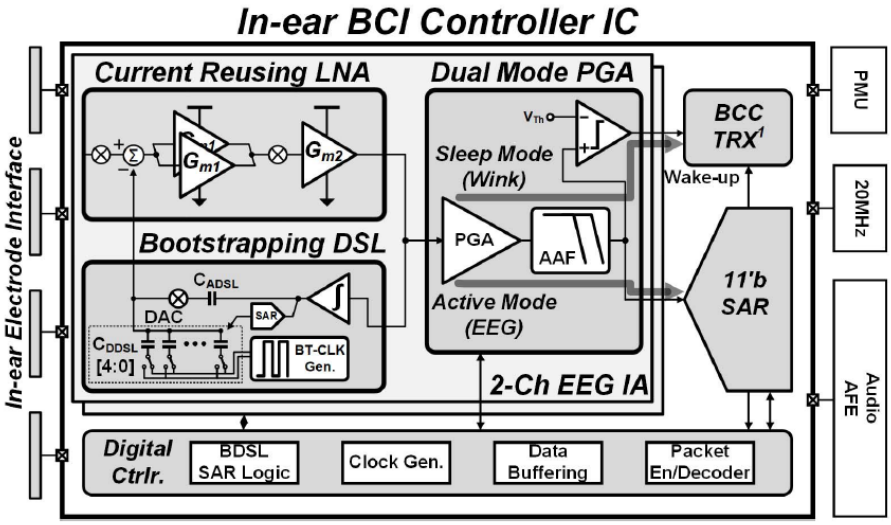

Figure 2.7: Block diagram of the integrated circuit designed by Lee et al..
Source: Adapted from [4]

3

Design of the first prototype

3.1. Selection of parts

Based on the findings in Chapter 2, a set of system requirements has been compiled. The requirements have been split up into quantitative and qualitative requirements. Table 3.1 lists the quantitative requirements and Table 3.2 lists the qualitative requirements.

Table 3.1: Quantitative system requirements.

Name	**Specification**	**Value**	**Comments**
QT1	Common-mode rejection ratio	>80 dB	The CMRR must be high enough to prevent distortion of the EEG signal as a result of common-mode interference.
QT2	Input referred noise	<2 μV_{pp}	The input referred noise level must be below the minimum magnitude of the EEG signals.
QT3	ADC resolution	≥ 8 bits	The minimum resolution to achieve a dynamic range of 2 μV_{pp} - 100 μV_{pp}, the typical magnitude range of EEG signals. If the DC offset and power line interference are not removed before the input of the ADC, the resolution should be higher, as the upper limit of the dynamic range should then be increased to include the interfering signals, while the lower limit does not change.
QT4	ADC sampling rate	>200 Hz	The minimum sampling rate to cover the entire frequency range of EEG signals (0.5 Hz-100 Hz).
QT5	Power consumption	<100 mW per earpiece	The total combined power consumption must be low enough to allow for 24-hour operation on a single battery. The intended division of the power budget can be found in Table 3.1.
QT6	Volume	<4 cm^3	The volume of the electronics must be small enough to fit into an earpiece.

Table 3.2: Qualitative system requirements.

Name	Requirement
QL1	The DC component of the acquired signals must be dealt with, to prevent saturation of the amplifier as a result of DC electrode offset.
QL2	The prototype must have a processing unit capable of executing simple machine learning algorithms.
QL3	The prototype must be easily re-programmable.
QL4	The extracted EEG information must be wirelessly transmitted.
QL5	The impedance of the electrode interfaces should be measurable by means of the recording device.

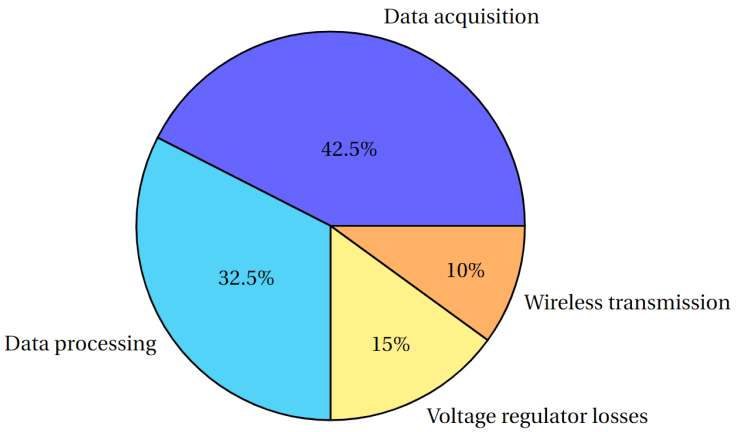

Figure 3.1: The intended division of the power budget.

Using these requirements a selection can be made of components to be used in the design.

subsectionAnalog-front-end Because a small form factor is required, components are desired that perform more than one function. Analog-front-ends (AFE) are an attractive option, as they combine amplification functionality with analog-to-digital conversion. Often extra features are included, like impedance measurement functionality. Some commercially available AFEs are considered for use in EEG recording. These are the ADS1299, produced by Texas Instruments [28], the ADAS1000-1, produced by Analog Devices [29], and the HM301D, produced by ST [30]. A comparison of the AFE specifications is shown in Table 3.3. The ADS1299 is chosen as the preferred AFE for this project, due to its superior input referred noise specification compared to its alternatives.

ADS1299

The Texas Instruments ADS1299 combines amplification and analog-to-digital conversion and is specifically designed for EEG and ECG recordings. It is available in four, six, and eight-channel variants. Each channel consists of a differential amplifier stage with a programmable gain between 1 and 24 and a 24-bit sigma-delta ADC. Using the sigma-delta ADC, noise shaping can be performed, allowing for low noise recording. The digitised signals are presented on an SPI bus. The sampling rate of the ADC can be set between 250 SpS and 16 kSpS, which allows for sampling of EEG signals above the Nyquist rate.

The maximum amplifier gain of 24 seems very low for an EEG amplifier. Because of the high ADC resolution of 24 bits, the EEG signals can be recorded without the need for a large amplifier gain. This does also allow for DC coupling to the amplifier, omitting the need for a high-pass filter before entering the amplifier. The ADS1299 is capable of measuring the small EEG signals, as well as the DC offset as a result of the high resolution.

The minimum input impedance of the ADS1299 is 1 GΩ or 500 MΩ when the lead-off functionality is used to monitor the state of the electrode connections. This lead-off functionality can be used in DC and AC mode.

Table 3.3: Specifications of the candidate analog-front-ends.

	ADS1299	**ADAS1000-1**	**HM301D**
CMRR @ 50 Hz (dB)	110	110	110
Input impedance (MΩ)	1000 (at DC)	1000 (at 10 Hz)	50 (0.05 Hz - 300 Hz)
Input referred noise (μV_{pp})	1 (0.01 - 70 Hz)	9 (0.05 - 150 Hz)	4.5 (0.1 -110 Hz)
Amplifier gain (V/V)	1 - 24	1.4 - 4.2	8 - 64
Number of bits	24	14	16
Sampling rate (SpS)	250 - 16k	1.024 M/2.048 M	2 M
Coupling	AC/DC	AC	AC/DC
Impedance measurement	DC & AC	DC & AC	DC & AC

In DC mode, a DC stimulus is used. A binary output signal is created, indicating whether the electrode makes a proper connection or not. In AC mode, an AC signal is used of a frequency inside the frequency band of interest. Two frequencies can be chosen, namely 7.8 Hz and 31.2 Hz. This signal is passed through the electrodes of a channel and subsequently measured. The electrode impedance can then be calculated using the measured signal voltage. These in-band measurements can only be performed when no EEG recording is performed. Continuous impedance measurement is possible, although this does require the addition of an AC source or sink of the desired frequency, connected externally to the input channels.

The amplifiers used in the ADS1299 have a common-mode rejection ratio of 110 dB. Together with the biasing circuit, used to reduce the common-mode signal present at the input electrodes, this will ensure that the common-mode signal still present at the input electrodes will not distort the measured signal. The input referred noise of the ADS1299 is 1 μV_{pp}, which is sufficiently low for the recording of EEG signals.

The ADS1299 can be operated in two main configurations. In the first configuration, electrode pairs are used for EEG measurements, with each electrode pair connected to its own channel. In the second configuration, all electrode channels are referenced to the same reference electrode. The reference electrode can internally be connected to the input of the differential amplifiers.

With all the combined functionalities of the ADS1299, many of the system requirements are satisfied. The amplifier-ADC combination allows for direct EEG recording, without the need for an additional amplifier stage or a high-pass filter to remove any DC component due to the high 24-bit resolution of the ADC. This omits the need for a high-pass filter at the input. The high common-mode rejection ratio in combination with the biasing circuitry prevents the common-mode signal from distorting the differential EEG signal. The sample rate of the Sigma-Delta ADC is sufficiently high to easily cover the entire frequency range of EEG, and noise shaping means that quantisation noise is low for the low frequencies of the EEG signal. With a maximum power consumption for the 8-channel version of the ADS1299 of 43 mW, the chip is suitable for operation using a battery. A block diagram of the ADS1299 can be found in Appendix B.1].

3.1.1. Wireless System-on-Chip

As mentioned in Section 2.3, there are two options when it comes to the wireless transmission of the recorded EEG signals. The first option is to transmit the entire data stream. This does mean that a large amount of data needs to be transmitted wirelessly, which can result in high power consumption. Another option is to perform some processing steps before wireless transmission takes place. If the size of the data stream is reduced enough by these processing steps, this can actually lead to a reduction of power consumption [31].

Several different Systems-on-Chip (SoC) are available that provide a combination of processing and wireless transmission capabilities. The main requirements when choosing a suitable SoC for the prototype are power consumption and processing power. SoCs have been considered produced by Nordic Semiconductors, Texas Instruments, NXP, and Silicon Labs. An overview of their specifications is shown in Tables A.1, A.2, A.3 and A.4 respectively. From these SoCs, the nRF5 range, produced by Nordic Semiconductors, has proven to be the most attractive due to the combination of high power efficiency and processing power it offers.

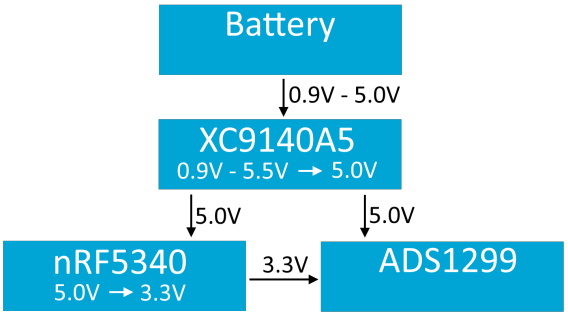

Figure 3.2: Schematic overview of the power system.

Nordic Semiconductors nRF5 range [32]
The nRF5 range of SoCs, produced by Nordic Semiconductors is made up of Bluetooth Low Energy SoCs. All the SoCs in the range feature Bluetooth Low-Energy functionality and many different interfacing protocols, like SPI, I2S, and UART. The SoCs differ when it comes to the CPU and memory. The nRF5340, the flagship of the range, includes a 128 MHz ARM Cortex-M33 with 1 MB flash memory and 512 kB RAM as the primary CPU. A second 64 MHz Arm Cortex-M33 CPU with 256 kB flash memory and 64 kB RAM is also included. Besides Bluetooth Low-Energy, the nRF340, nRF52840, nRF52833, and nRF52820 also support Zigbee. A complete overview of the different configurations inside of the nRF5 range is given in Table A.1.

To quantify the power efficiency of the SoCs, CoreMark/mA is used. CoreMark is a benchmarking system for SoCs, where a higher score means better processing capabilities. Table A.1 shows the CoreMark/mA for the entire nRF5 line, as well as the CoreMark score. It should be noted that all SoCs used a 3 V supply voltage during the benchmark. From the CoreMark/mA scores, it becomes clear that the nRF5340 can provide the most processing performance per unit of power. This makes it an attractive option, as it combines the highest power efficiency with the highest total processing power in the range. Additionally, the Cortex-M33 that is used in the nRF5340 includes a dedicated digital signal processing unit, as well as a floating-point unit, enabling efficient data processing. Many different digital signal processing instructions are available, including filtering functions and transform functions, which are likely to be useful for EEG applications.

The nRF5340 exceeds the second most powerful wireless SoC currently available by more than 200 CoreMark. The high processing power of the nRF5340 enables it to run edge machine learning algorithms, which is not possible with its less powerful alternatives. With a CoreMark/mA of 101, the nRF5340 is the second most efficient wireless SoCs currently available, only surpassed by the EFR32BG22 range by Silicon Labs. Overall, the nRF5340 seems to be the most attractive package, combining the highest processing power with high efficiency. Because of this, the nRF5340 is chosen to be used in the prototype.

3.1.2. Power system

To power the ADS1299 and nRF5340, two different voltages are required. The analog part of the ADS1299 uses a 5 V operating voltage, while the digital operating voltage of the nRF5340 is 3.3 V. The digital parts of the ADS1299 can operate at voltages ranging between 1.8 V and 3.6 V, meaning that the 3.3 V used by the nRF5340 can also be used for the ADS1299.

Because the prototype will be battery-powered, a 5.0V voltage regulator is included in the design, ensuring a consistent supply voltage. The Torex XC9140A5 is chosen for this purpose [33]. The XC9140A5 accepts an input voltage between 0.9 V and 5.5 V and converts it to an output voltage of 5.0 V. The conversion efficiency ranges between 80% and 90% for output currents higher than 1 mA.

The nRF5340 accepts a 5 V supply voltage when using the VDDH pin. The 5 V input voltage is internally converted to 3.3 V, which then is used to power the rest of the device. In this setup, the VDD pins of the nRF5340 can be used to power external devices. The digital parts of the ADS1299 can therefore operate using the voltage supplied by the nRF5340. Figure 3.2 shows a schematic overview of the power system.

The worst-case power consumption can be calculated, based on the peak power consumption of the included devices. As mentioned in Section 3.1, the maximum power consumption of the 8-channel ADS1299 is equal

to 43 mW. The nRF5340 has a power consumption of 50.7 mW when operating at the full capacity of the CPU and transmitting using Bluetooth Low-Energy at a rate of 1 Mbps [32]. Combining the power consumption of the two ADS1299 chips and the nRF5340 results in a maximum power consumption of 136.7 mW. Taking into account the worst-case conversion efficiency of 85% of the XC9140A5 yields an effective maximum total power consumption of 160.8 mW. In practice, the average power consumption of the prototype will likely be lower, as the individual components will not continuously be operating at peak power.

3.2. System design

3.2.1. System configuration

The choice is made to make use of all eight input channels provided by the ADS1299. The ADS1299 will be used in referential mode, meaning that all electrodes will be measured with respect to the same electrode instead of in differential pairs. In the referential configuration, it is also possible to retrieve the differential signal between the measuring electrodes, as they are measured with respect to the same reference.

The data rate of the ADS1299 will be set at 250 SpS. This data rate is high enough to cover the frequency band of interest (0.5 Hz-100 Hz) while keeping the data stream that needs to be processed and transmitted as small as possible. The amplifier gain is set to 24. A maximum signal magnitude of 187.5 mV can be measured in this configuration, with an input-referred noise of 1 μV_{pp}.

Most of the existing in-ear EEG implementations use a single earpiece. As discussed in Section 2.5.1, a single ear setup limits the distance between the measuring and reference electrodes, resulting in recorded EEG signals of small magnitude. A two-ear setup is proposed, to increase the magnitude of the recorded signal. By referencing the electrodes from one earpiece to a reference electrode in the other earpiece, the distance between the measuring and recording electrodes is increased. This is expected to increase the magnitude of the recorded EEG signals. The experiments conducted in Chapter 6 refute this. A configuration selector has been included to allow each earpiece to either be referenced to the same ear or the opposite ear. A schematic of the proposed two-ear setup is shown in Figure 3.3.

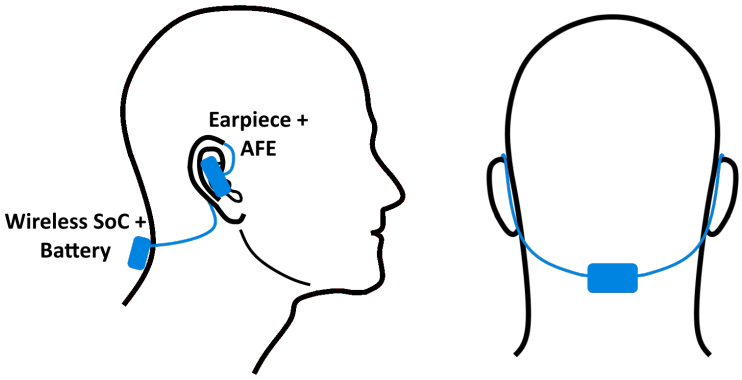

Figure 3.3: The proposed two-ear setup.

This two-ear setup consists of three modules: the microcontroller module, containing the nRF5340 and the battery, and two earpiece modules, containing the ADS1299. The ADS1299 are placed on their own dedicated PCBs, instead of together with the nRF5340, to make the wires carrying the analog EEG signals as short as possible. This is done to reduce the interference that is picked up by the wires. The wires connecting the earpiece modules to the microcontroller module only carry digital signals, for which interference will not pose a problem. These wires contain the SPI connections and the connections needed to power the ADS1299. Two wires are also present, connecting the reference electrode from one earpiece to the other earpiece. These are long wires carrying analog signals, making them susceptible to interference. The wires are included to see if using a reference electrode placed at the opposite ear increases the quality of the recording, despite the higher susceptibility to interference. The wire can be disconnected from the reference electrode terminal by using the configuration selector.

3.2.2. PCB design

Microcontroller PCB

The microcontroller PCB, containing the wireless SoC and power system, acts like the main hub of the system, connecting to the PCBs at both of the earpieces. The schematics of the design are shown in Appendix C.1.1. Instead of using the standard nRF5340, the choice has been made to use the Nora B106. The Nora B106 incorporates the nRF5340 but also contains all components required for operation, as well as an integrated antenna [34].

Pins are included for the programming and debugging of the device using the Serial Wire Debug (SWD) protocol. A Universal Asynchronous Receiver-transmitter (UART) interface is also included. Besides this, the option is added to power the PCB using an external power supply, bypassing the voltage regulator. A switch can be used to select either battery operation mode, or operation using the external power supply. These additional functions are mainly introduced to allow for easy debugging of the device during development.

Based on the schematic, a PCB design has been made. The design is shown in Figure 3.4.

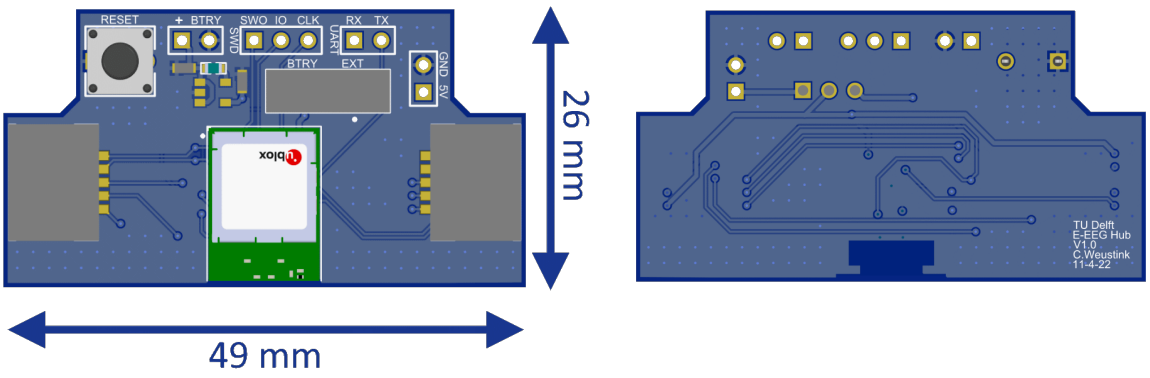

(a) Front

(b) Back

Figure 3.4: The design of the main PCB.

Cutouts have been made, removing parts of the PCB that contained no components, resulting in a more compact design. The dimensions of the PCB are small enough to not cause discomfort when placed in the neck of the user.

Earpiece PCBs

The earpiece PCBs contain the ADS1299 and additional components it requires for operation. The schematics of the design are shown in Appendix C.1.2. Each of the positive terminals of the input channels features a passive low-pass filter, consisting of a series 5 kΩ resistor and a 4.7 nF capacitor connected to the reference electrode terminal. This low-pass filter is put in place to prevent aliasing during the sampling of the EEG signals. The input channels and the bias terminal are connected to solder pads, to which the electrodes can be connected.

All inputs and outputs of the ADS1299 that need to be accessed by the wireless SoC are connected to solder pads. This includes the pins needed for SPI communication: DRDY, SCLK, DIN, DOUT, and CS'. Besides this, the analog and digital supply voltages and ground are connected through the solder pads.

The first prototype has been designed with testing in mind. Header pins are included, allowing for operation in different configurations by placing jumpers in different positions. Including these header pins increases the size of the PCB, but the added functionality is deemed more important for the first prototype. Based on the test conducted with the first prototype, the most desirable configuration can be chosen, which can then be used in a more compact, less flexible prototype. The prototype PCB is shown in Figure 3.5.

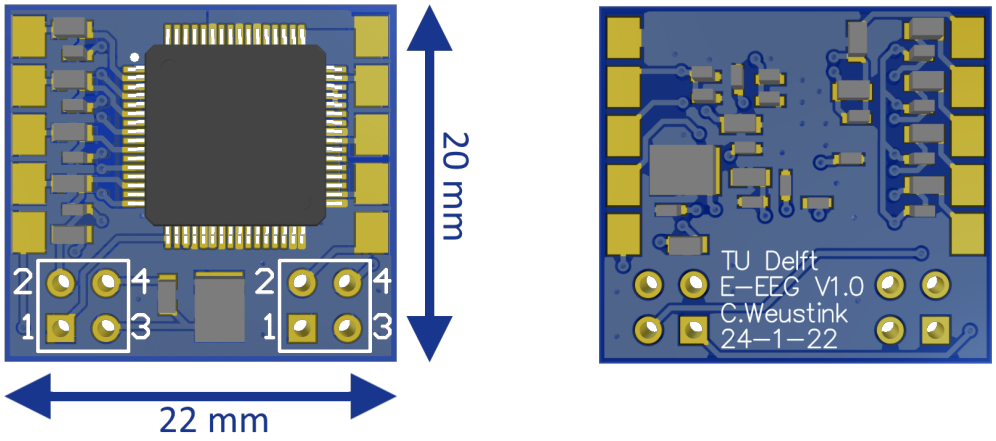

(a) Front

(b) Back

Figure 3.5: The design of the first prototype PCB.

Using the header pins, two different referencing configurations are available: In the first configuration, the reference electrode connected to the PCB is routed to a solder pad. This can be used to connect the reference electrode to a second PCB. In turn, the reference electrode from another PCB is received via another solder pad, connected to the input of the ADS1299. This configuration is used in the two-ear setup, as explained in Section 3.2.1. In the second configuration, the reference electrode is routed to the input of the ADS1299 on the PCB itself, allowing for operation in a one-ear setup.

In both these configurations, two options are available. The first option is to connect the reference electrode to the input of the ADS1299 as normal. The second option is to pass the reference electrode through a low-pass filter first. The idea behind this is that all signals within the bandwidth of EEG (0.5 Hz - 100 Hz) are filtered out, leaving only a DC reference signal. This is mainly thought to improve operation in a one-ear setup, as cancellation of similar signals is prevented. The idea behind this is further explained in Appendix D. It did not work out as intended in practice. An overview of the jumper positions to achieve the different configurations is shown in Figure F.1.

3.2.3. Assembly

As the result of the global chip shortage at the time of this project, the 8-channel version of the ADS1299 analog front-end was not available. Because of this, the 4-channel version has been used instead. As both versions are completely pin-compatible, this does not require a redesign of the earpiece PCBs. It does mean that each of the earpieces will only be able to record 4 channels, instead of 8.

Figure 3.6 shows the assembled microcontroller PCB.

Figure 3.6: The assembled microcontroller PCB.

Figure 3.7 shows the assembled earpiece PCB. The figure shows a red wire that is not part of the intended

design. The wire connects the active-low RESET and PWDN pins of the ADS1299 to VDD via a 10 kΩ resistor. This is required, as no internal pull-up resistor is included in the ADS1299 and the pins are left floating in the PCB design, causing the ADS1299 to be in the powered-down state. The wire mitigates this problem externally.

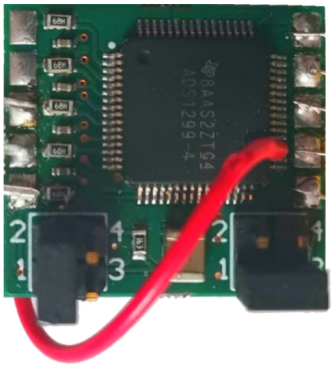

Figure 3.7: The assembled earpiece PCB.

The microcontroller PCB is connected to the earpiece PCBs by 2 connectors with 10 wires each. Heat-shrink tubing is used to keep the wires together. Figure 3.8 shows the earpiece PCBs connected to the microcontroller PCB.

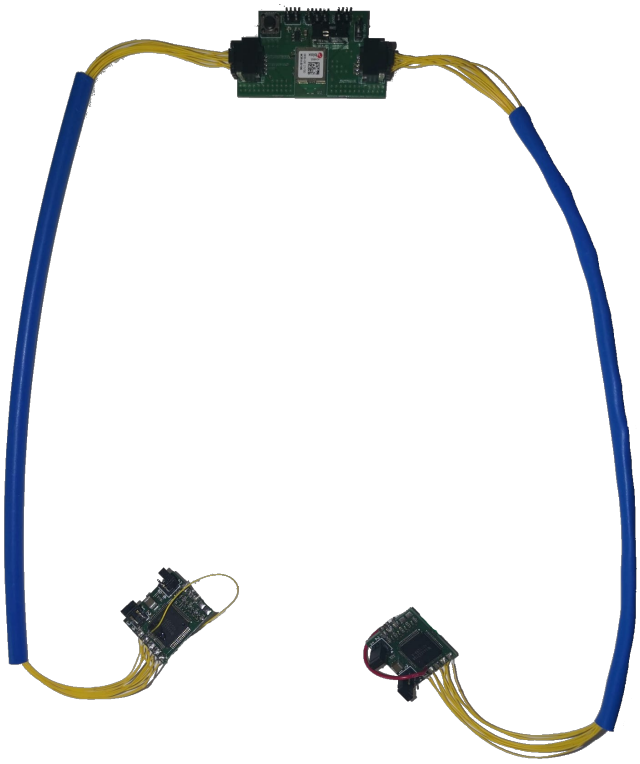

Figure 3.8: The assembled prototype.

One minor issue has been found with the prototype assembly. Sometimes the connection between the microcontroller and earpiece PCBs becomes unstable at the connectors when the prototype is moved around. This can result in a failed recording. In a future prototype, this issue can be avoided by using a soldered connection between the microcontroller and earpiece PCBs. Doing this removes the possibility of disconnecting the

earpiece PCBs from the microcontroller PCB, but will increase the reliability of the device. With the current prototype, a short test recording can be made to validate that the PCBs are properly connected.

3.2.4. Programming the prototype

The most convenient way to program the nRF5340 is by using the nRF5340 development kit [35]. The nRF5340-DK gives access to all the pins of the nRF5340 and includes a debugger. The board can be connected to a PC using a micro-USB cable, which both powers the board and can be used for programming the nRF5340-DK. The nRF5340-DK allows for programming external targets using a dedicated connector, which can be used to program the chip that will be used on the prototype. The programming of the prototype is further elaborated upon in Appendix G.

4

Prototype performance

4.1. Prototype specifications

The input channels of the prototype are all connected together with the bias electrode to measure the input-referred noise. A one-minute recording is made in this configuration. During the recording, a maximum signal amplitude of 0.57 μV_{pp} is measured for all four channels. This satisfies the 2 μV_{pp} requirement. Figure 4.1 shows the signal magnitude spectrum of the recording between 0.5 Hz and 100 Hz.

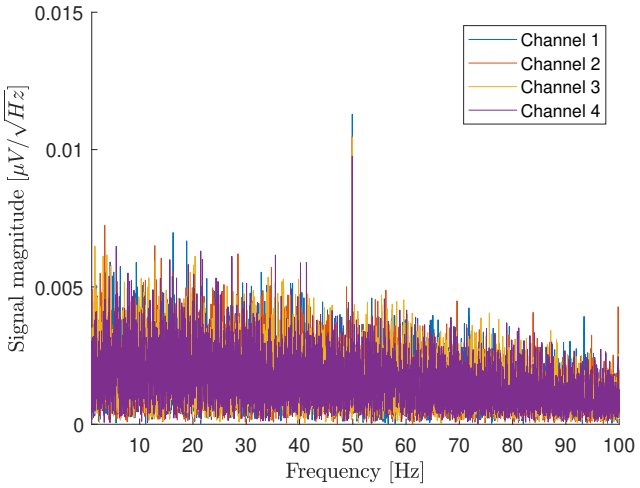

Figure 4.1: The amplitude spectrum of the prototype, with all inputs connected to the bias electrode.

Each channel shows a peak at 50 Hz as the result of power line interference. No other peaks are present that could indicate a source of interference on the prototype itself, as no large peaks are visible that are shared between all channels. The magnitude spectra are similar between all channels.

The power consumption of the prototype is measured in different configurations. Table 4.1 shows an overview of these measurements.

Table 4.1: The average and peak power consumption of the prototype in different configurations.

Connected earpiece PCBs	Idle	Average active	Peak Active
0	26 mW	28 mW	31 mW
1	51 mW	60 mW	65 mW
2	75 mW	87 mW	96 mW

Table 4.1 shows the average and peak power consumption while the prototype is recording and wirelessly transmitting the recorded data. The idle power consumption has also been measured. This is measured while the prototype is not recording. The measurements show that each AFE adds 30 mW to the average power consumption when active, with the microcontroller PCB consuming 28 mW when not connected to the earpiece PCBs. The idle power consumption is not much lower than the power consumption when active. The idle power consumption could be decreased by putting the ADS1299 in the powered down state when the prototype is not active. This can be done by altering the device firmware. The average power consumption in active mode, with 2 earpiece PCBs connected, is 87 mW. This is below the limit of 100 mW per earpiece, set in the system requirements.

The common-mode rejection ratio is also measured for each of the input channels. To do so, a 1 V_{RMS} sine-wave is presented to the reference and measuring electrode channels, with respect to the bias electrode. This is done at 50 Hz and 60 Hz, as power line interference is expected at these frequencies. Table 4.2 shows the results from these measurements. The table shows the CMRR of the worst-performing channel.

Table 4.2: The measured common-mode rejection ratio for the first prototype.

Frequency	**Input signal**	**Measured signal**	**CMRR**
50 Hz	1 V_{RMS}	84.8 μV_{RMS}	81.43
60 Hz	1 V_{RMS}	96.5 μV_{RMS}	80.31

The measured CMRR is above the 80 dB lower limit set in the requirements, but is lower than expected, as the CMRR of the ADS1299 is advertised to be above 110 dB. A possible cause of the decrease in the CMRR is that the shunt 4.7 nF capacitor in the input filter reduces the input impedance of the analog front-end for higher frequencies. This increases the effect of input impedance mismatch, turning common-mode signals into differential-mode signals, which leads to a degraded common-mode rejection ratio. This theory is supported by a CMRR measurement performed at 1 Hz. The measured CMRR at 1 Hz is equal to 100.92 dB, showing that the CMRR indeed decreases at higher frequencies.

An overview of the prototype specifications is shown in Table 4.3.

Table 4.3: Overview of the prototype specifications.

Prototype specifications	
Number of channels	8 (4 simultaneously)
Input-referred noise	0.57 μV_{pp}
Common-mode rejection	>80 dB @ 50 Hz
Input impedance at DC	1 GΩ
ADC resolution	24 bits
ADC data rate	250 SpS
Average power dissipation	87 mW

4.2. Paradigm performance

To verify the functionality of the prototype, it is tested using the auditory steady-state response, steady-state visual evoked potential, and alpha-band modulation paradigms, as elaborated upon in Section 2.5.1 The experiments are also performed using the commercially available OpenBCI Cyton Biosensing Board, to be used as a reference [36]. The OpenBCI Cyton Biosensing Board is a wireless EEG recording device, meant for use with one of the OpenBCI scalp recording products. As the in-ear electrodes are not yet completed at this stage of the project, the OpenBCI Ultracortex Mark IV scalp EEG recording headset [37] is used for the experiments. Figure 4.2 shows an image of the headset, as well as the used electrode numbering system.

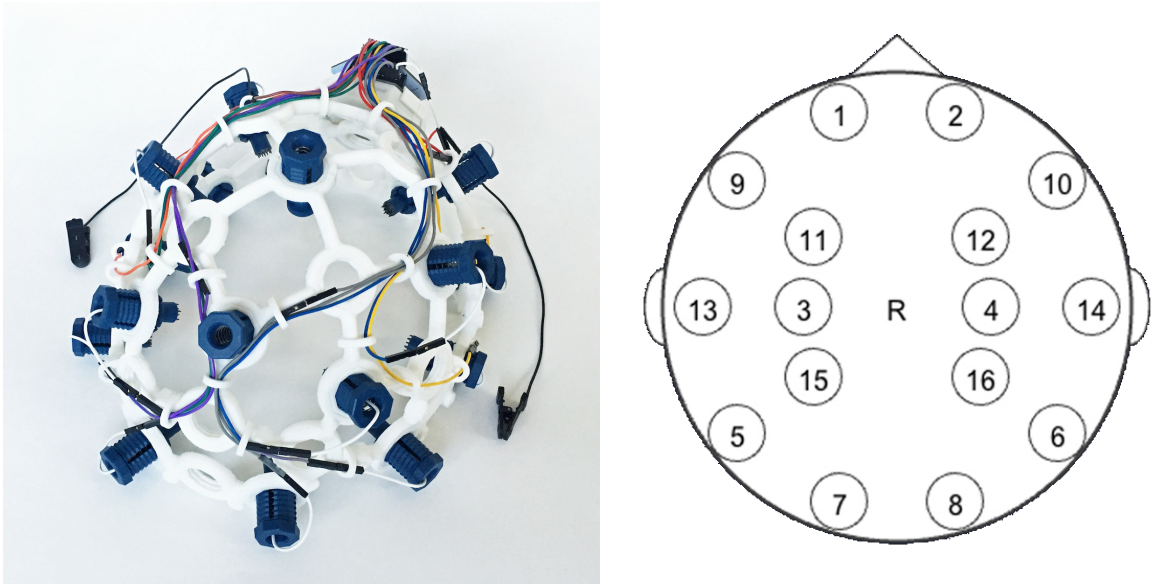

(a) Headset

(b) Electrode numbering system

Figure 4.2: The OpenBCI Ultracortex Mark IV EEG recording headset used in the experiments. Source: Adapted from [37]

The Ultracortex Mark IV features dry, comb-shaped electrodes, as well as two dry ear-clip electrodes for the reference and bias. By using the same electrodes with both the Cyton Biosensing Board and the prototype, the influence of the electrodes on the recording performance is removed, making for a fair comparison between the devices.

For both devices, each experiment is conducted 10 times with the reference electrode connected to the left ear and ten times with the reference electrode connected to the right ear, making a total of 20 experiments per device. The bias electrode is connected to the opposite ear of the reference electrode in each experiment. The software used in these experiments is elaborated upon in Appendix G.3.

4.2.1. Auditory steady-state response

A Gaussian white noise signal is amplitude modulated using a sine wave of 40 Hz and a modulation depth of 100 %. While performing an EEG recording, the audio signal is presented to the subject for 120 seconds. Electrode location 2 is used during the experiments, as this location provided the largest response. Figure 4.3 shows the power spectra from the experiments, as well as the average of the power spectra in blue.

A clear peak is visible at 40 Hz in each of the experiments. Table 4.4 shows the signal-to-noise ratio for each of the experiments, as well as the average signal-to-noise ratio for each of the configurations. Here, the signal-to-noise ratio is calculated by dividing the signal power at the peak by the average signal power in the frequency band between 35 Hz and 45 Hz, excluding the peak itself:

$$\text{SNR} = 10 \cdot \log_{10}\left(\frac{P_{peak}}{P_{35-45Hz}}\right). \tag{4.1}$$

The table shows a slightly higher average signal-to-noise ratio for the experiments conducted with the Cyton Biosensing board than for the prototype. This difference could be down to the limited amount of conducted experiments. This is reflected in the standard deviation of the experiments. The results do show that the auditory steady-state response can reliably be detected with the prototype.

In the power spectra, shown in Figure 4.3, large peaks occur at 31 Hz in the experiments conducted with the Cyton Biosensing board. These peaks do not occur at a harmonic of the modulation frequency (40 Hz), or the frequency of the power line interference (50 Hz). The peaks are not present in the experiments conducted with the prototype. A possible explanation for this could be that the Cyton Biosensing board uses a 31 Hz signal internally, which interferes with the recording.

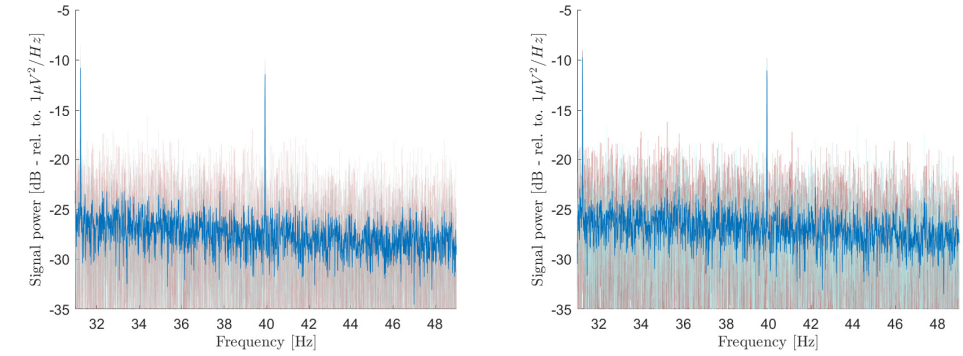

(a) Cyton board - reference left ear

(b) Cyton board - reference right ear

(c) Prototype - reference left ear

(d) Prototype - reference right ear

Figure 4.3: Power spectra of the ASSR experiments.

Table 4.4: Signal-to-noise ratios for each of the ASSR experiments.

	SNR (dB)			
Device	**Cyton Biosensing Board**		**Prototype**	
Reference electrode side	**L**	**R**	**L**	**R**
Experiment 1	16.07	14.63	15.73	16.84
Experiment 2	14.66	14.18	10.08	14.16
Experiment 3	15.97	17.03	15.11	10.41
Experiment 4	18.63	17.12	14.67	16.42
Experiment 5	14.81	16.42	14.05	15.72
Experiment 6	13.69	16.01	12.29	12.74
Experiment 7	10.42	17.33	12.72	15.14
Experiment 8	16.66	16.38	12.52	12.56
Experiment 9	18.95	17.11	17.56	14.74
Experiment 10	18.10	16.19	15.06	15.47
Average	**15.80**	**16.24**	**13.979**	**14.42**
Standard deviation	**2.44**	**1.01**	**2.01**	**1.89**

4.2.2. Steady-state visual evoked potential

Stimulation is performed using a square on a laptop display, changing colour between black and red at a rate of 10 Hz. A 60-second EEG recording is made while the subject is looking at the flashing square. Electrode location 7 is used during the experiment, as this location showed the largest response. Figure 4.4 shows the power spectra of the experiments. In the figures, the power spectra of all experiments are overlapped. The average of the power spectra is shown in blue.

In all experiments, a clear peak is visible at 10 Hz. The signal-to-noise ratio of each of the experiments is shown in Table 4.5, as well as the average signal-to-noise ratio per configuration. Here the signal-to-noise ra-

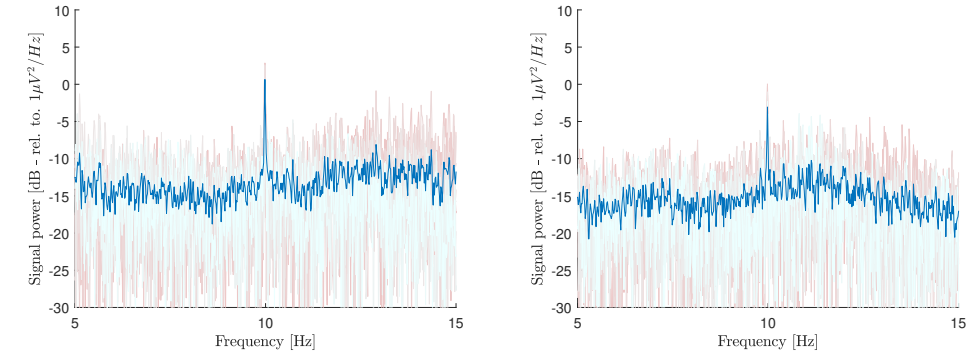

(a) Cyton board - reference left ear

(b) Cyton board - reference right ear

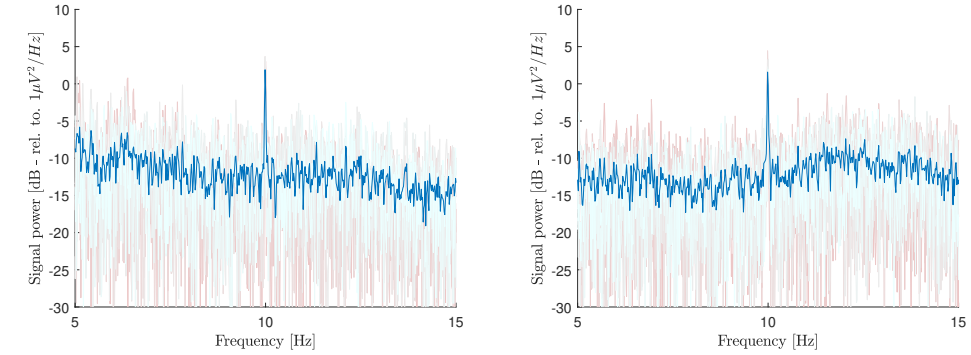

(c) Prototype - reference left ear

(d) Prototype - reference right ear

Figure 4.4: Power spectra of the SSVEP experiments.

tio is defined as the signal power at the peak (10 Hz), divided by the average signal power in the neighbouring frequencies, ranging between 5 Hz and 15 Hz:

$$\text{SNR} = 10 \cdot \log_{10}(\frac{P_{peak}}{P_{5-15Hz}}). \tag{4.2}$$

Table 4.5: Signal-to-noise ratios for each of the SSVEP experiments.

	SNR (dB)			
Device	**Cyton Biosensing Board**		**Prototype**	
Reference electrode side	**L**	**R**	**L**	**R**
Experiment 1	15.94	14.85	16.54	10.60
Experiment 2	12.82	13.61	13.07	14.59
Experiment 3	16.00	12.54	13.37	13.01
Experiment 4	12.58	10.01	15.91	16.87
Experiment 5	14.69	5.94	17.07	12.17
Experiment 6	12.77	15.13	13.75	15.78
Experiment 7	10.59	8.91	13.23	15.55
Experiment 8	11.71	7.30	10.28	13.58
Experiment 9	14.68	11.12	11.41	13.25
Experiment 10	9.81	13.07	10.21	11.97
Average	**13.16**	**11.25**	**13.484**	**13.737**
Standard deviation	**2.02**	**2.99**	**2.32**	**1.85**

The table shows that the signal-to-noise ratio, in the configurations with the reference electrode placed at the left ear, is comparable between devices. With the reference electrode placed at the right ear, a larger

difference can be seen between the devices. The average signal-to-noise ratio is in this case smaller for the Cyton board than for the prototype. This difference is caused by the larger spread in signal-to-noise ratios between experiments for the Cyton biosensing board. Some experiments showed a much lower signal-to-noise ratio than the others, reducing the average. This is reflected in the relatively high standard deviation for the experiments in this configuration.

4.2.3. Alpha-band modulation

The alpha-band modulation experiment is conducted by doing simple arithmetic for 15 seconds (focused phase) and then relaxing with closed eyes for 15 seconds (relaxed phase). An increase in signal power in the alpha-band (8-12 hertz) is expected in the relaxing phase with respect to the focused phase. For the experiment, electrode 8 of the Ultracortex Mark IV headset is used, as alpha waves were best detected at this channel for both devices. Figure 4.5 shows the signal power in the alpha band (8-12 Hz) during the experiments.

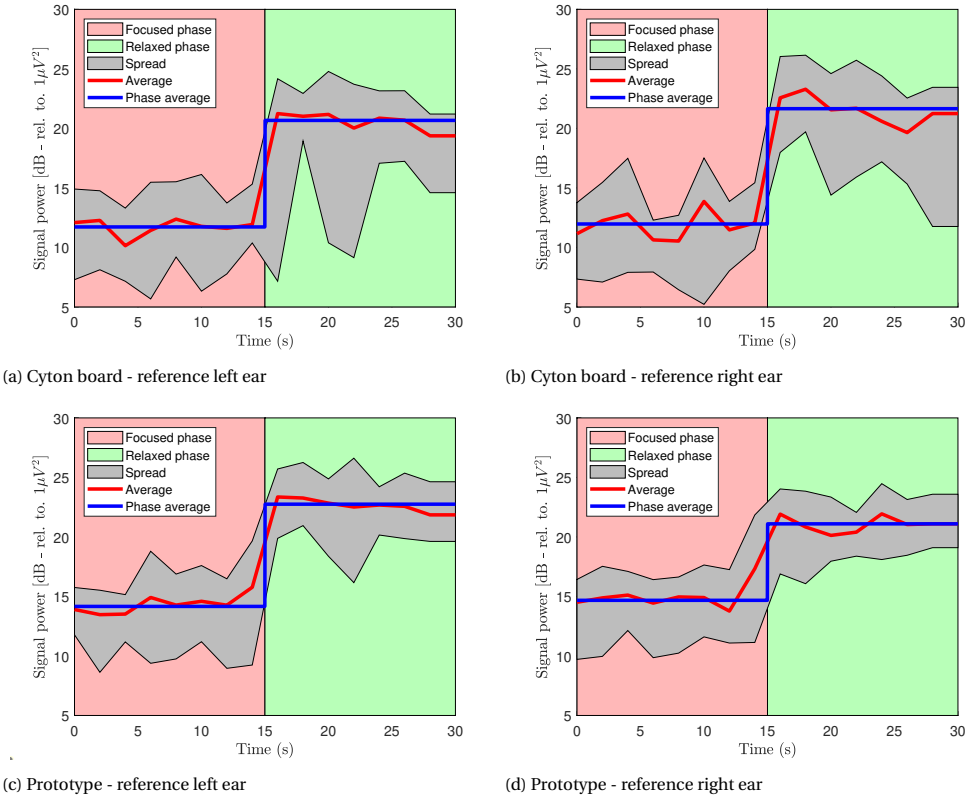

(a) Cyton board - reference left ear

(b) Cyton board - reference right ear

(c) Prototype - reference left ear

(d) Prototype - reference right ear

Figure 4.5: Power in the alpha band for the different configurations.

The figure shows a clear increase in alpha-band power in the relaxing phase compared to the focused phase for both devices. Table 4.6 shows the increase in the phase average between the focused and relaxed phases for each configuration.

In the experiments, the average increase in alpha waves between the phases is higher for the Cyton board than for the prototype in both configurations. When looking at Figure 4.5, it is clear that the alpha-band signal power in the relaxed phase of the experiment is comparable between all configurations. In the focused phase, the average alpha-band power is lower for the experiments conducted with the Cyton board than for the recordings conducted with the prototype. A possible explanation for this can be that a higher amount of low-frequency interference is picked up by the prototype compared to the Cyton board. Another cause could be a worse electrode-skin connection in the experiments conducted with the prototype compared to those conducted with the Cyton board. Nevertheless, an increase in the signal power in the alpha-band has been measured in all of the experiments conducted with the prototype.

Table 4.6: The power increase in the alpha-band between the phases.

	Power increase (dB)			
Device	**Cyton Biosensing Board**		**Prototype**	
Reference electrode side	**L**	**R**	**L**	**R**
Experiment 1	8.75	10.37	7.41	6.05
Experiment 2	9.11	11.30	9.76	6.50
Experiment 3	8.57	9.95	10.21	6.73
Experiment 4	8.87	9.10	7.76	7.04
Experiment 5	9.38	11.28	9.60	7.17
Experiment 6	6.19	8.08	8.22	5.57
Experiment 7	10.54	7.61	7.76	5.89
Experiment 8	10.59	9.62	8.72	6.02
Experiment 9	8.68	9.86	7.96	6.58
Experiment 10	9.17	8.56	8.01	6.77
Average	**8.99**	**9.57**	**8.54**	**6.43**
Standard deviation	**1.16**	**1.19**	**0.93**	**0.50**

5

Final design

5.1. PCB design

Based on the tests done with the first prototype, some alterations are made to the design. The new design is shown in Figure 5.1, with the designs of the microcontroller and analog front-end PCBs in Figures 5.2 and 5.3 respectively. The PCB schematics can be found in Appendix C.2.

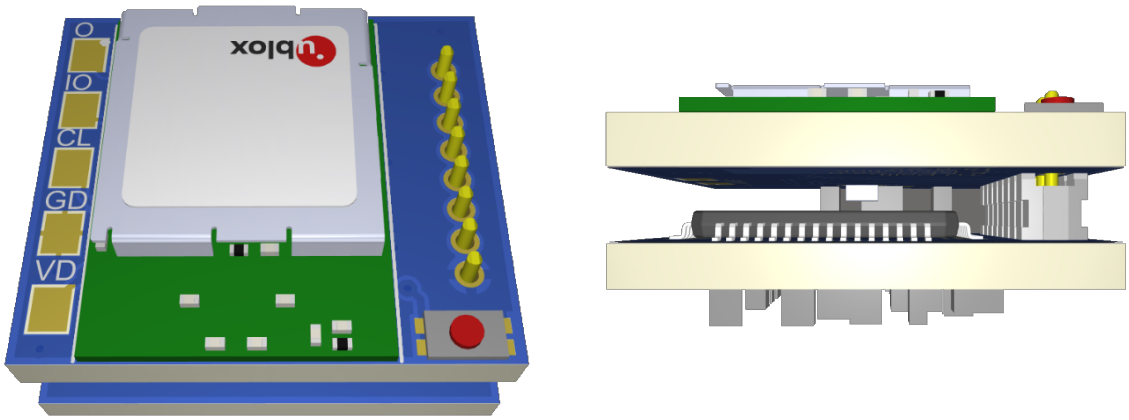

(a) Top

(b) Side

Figure 5.1: The final design.

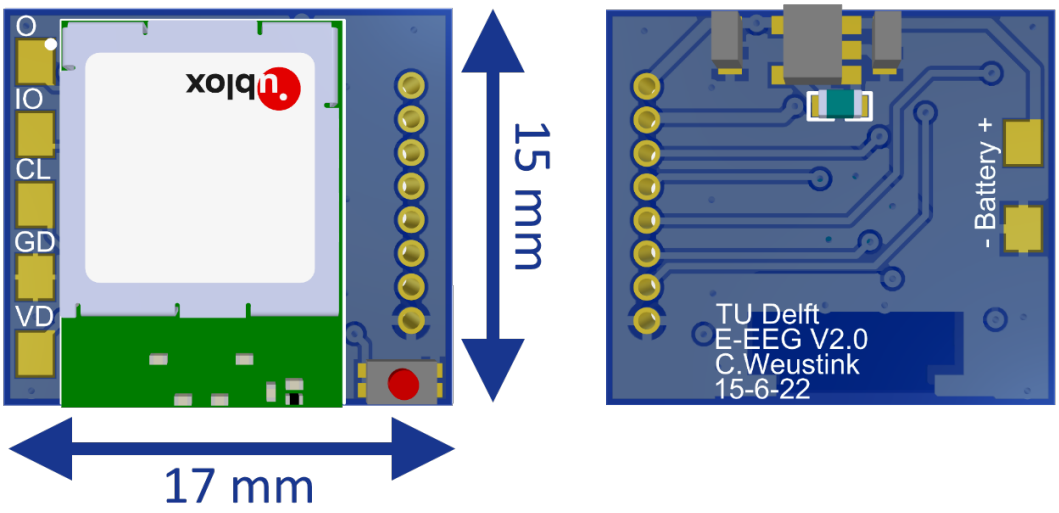

(a) Front

(b) Back

Figure 5.2: The design of the microcontroller PCB.

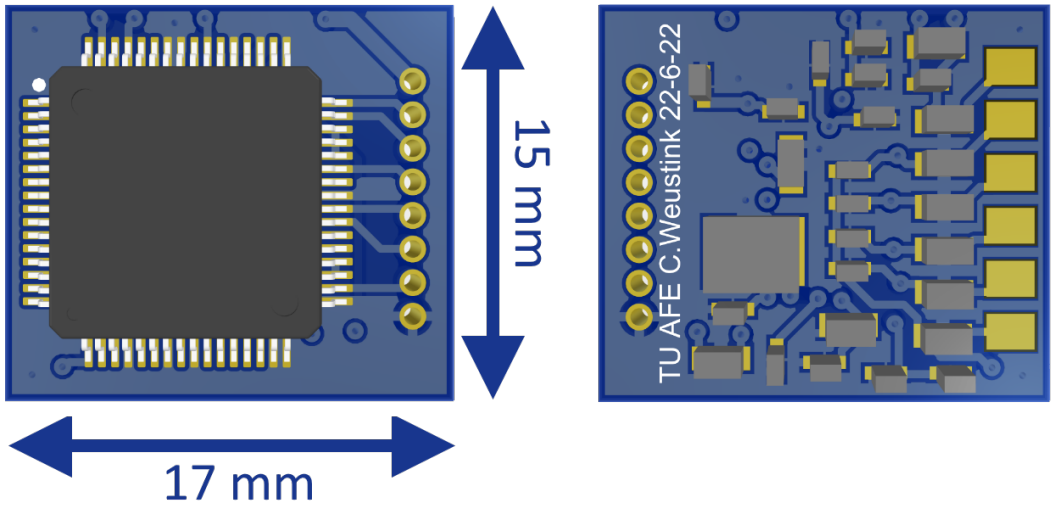

(a) Front

(b) Back

Figure 5.3: The design of the analog front-end PCB.

The analog front-end and microcontroller PCBs are combined into one module. The benefit of doing this is threefold. Firstly, the data throughput is increased. In the first prototype, one microcontroller was shared between two analog front-ends. This meant that the data from only four of the eight available channels could be transmitted simultaneously, as the BLE throughput using a single microcontroller was not sufficient to transmit all data at once. This issue was not expected beforehand, as the recorded data was planned to be processed on-board before wireless transmission, reducing the amount of data to be transmitted. As the data processing algorithms have not yet been implemented at this stage of the project, the choice has been made to transmit all of the recorded data instead, requiring higher throughput. The new design features a dedicated microcontroller for each earpiece, allowing the data from all channels to be transmitted simultaneously. Secondly, a more stable connection is created between the analog front-end and microcontroller. In the first prototype, each analog front-end is connected to the microcontroller PCB through a connector with 10 wires. Sometimes this connection is unstable, corrupting the recorded data. The final design uses eight soldered connections between the microcontroller and analog front-end, ensuring a stable connection. Lastly, the size of the design has been reduced. The connectors have been removed from the design and there

is no longer a need for a large number of wires.

The size is further reduced by stacking the analog front-end and microcontroller on top of each other, reducing the footprint of the design. The UART connections have been removed, previously in place for debugging purposes, and a smaller form-factor reset switch is used. These measures result in a final size of 17x15x8mm, satisfying the 4 cm^3 maximum volume requirement.

The module can be powered using the battery connections at the bottom of the microcontroller PCB. To facilitate the battery, a behind-the-ear design is proposed, as commonly used in hearing aids. This allows for a battery and power switch to be placed behind the ear of the user, with the PCBs placed on top of the in-ear electrodes. Figure 5.4 shows a schematic of the intended device setup, as well as a 3D model showing the scale of the components.

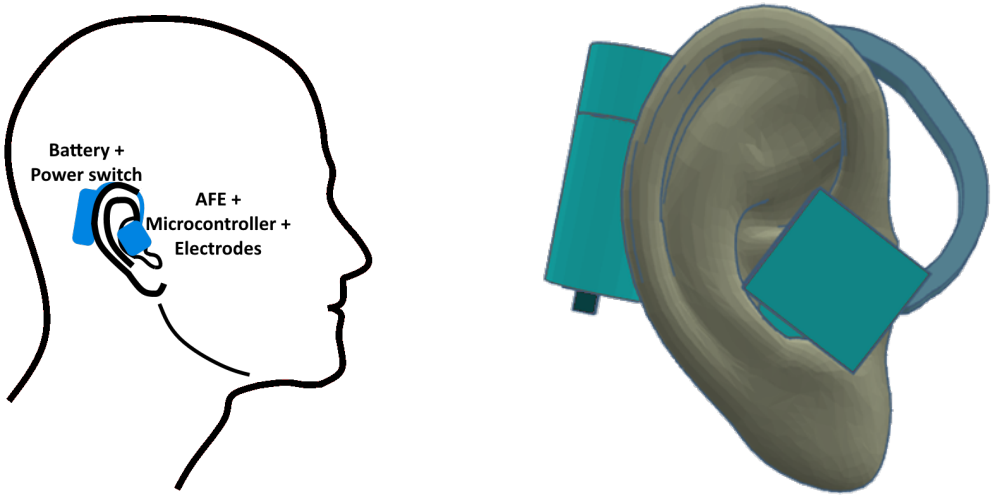

(a) System configuration

(b) 3D model

Figure 5.4: The intended setup of the device.

The average power consumption of the first prototype, with one analog front-end enabled, is equal to 60 mW. The power consumption of the new design is expected to be similar, as the same hardware configuration is used. A 1/2 AA lithium battery is a good candidate to power the device. With a >700 mAh capacity for high discharge rates, an operating voltage of 3.6 V and a maximum constant current of 50 mA, it is capable of powering an earpiece for more than 42 hours [38]. With a diameter of 14.5 mm and a length of 25 mm, it is small enough to be placed behind the ear.

Each earpiece is completely independent. This makes it possible to use either a single earpiece or one earpiece for each ear. During assembly, the choice can be made to connect the reference electrode of one earpiece to the analog front-end of another earpiece, creating the two-ear setup proposed in the first prototype. The reference electrode can also be connected to the analog front-end located at the same earpiece, resulting in a fully wireless design. To reduce the size of the design, the configuration selector that was present in the first prototype for this purpose has been omitted.

5.2. Assembly

The two PCBs could be assembled without issues. A piece of electrical tape has been placed on the analog front-end PCB, before soldering the microcontroller PCB on top using header pins. This is done to ensure the components on each of the PCBs are isolated from each other. Figure 5.5 shows the assembled prototype.

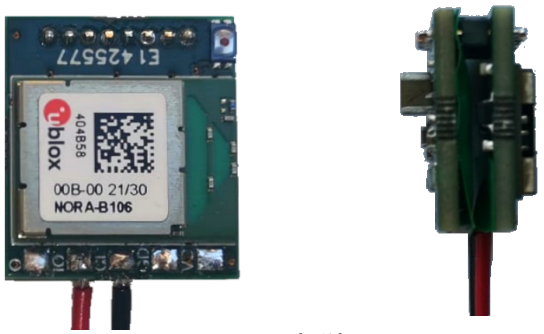

(a) Front

(b) Side

Figure 5.5: The assembled final prototype.

The new prototype design is significantly smaller than the first prototype, increasing the portability. Two wires are connected to the side of the prototype. These connect to the battery used to power the device. A comparison of the scale of the first and second prototypes is shown in Figure 5.6.

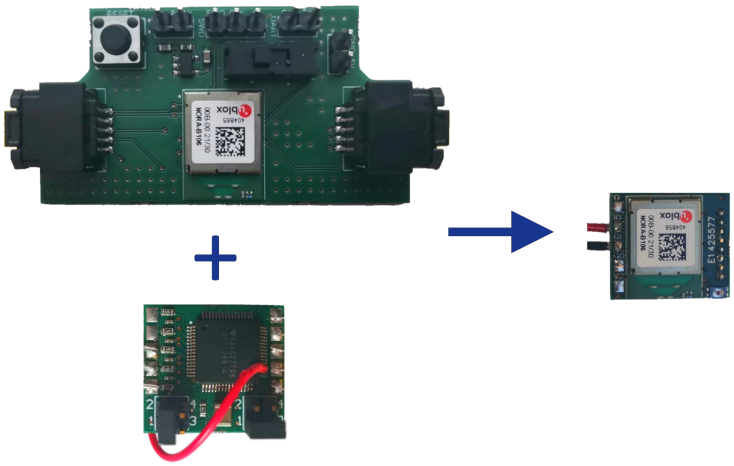

Figure 5.6: Scale comparison between the first prototype (left) and final prototype (right).

5.3. Prototype specifications

A one-minute recording is made with all input channels connected together with the bias electrode to measure the input-referred noise. During the recording, a maximum signal amplitude of 0.57 μV_{pp} is measured for all four channels, satisfying the 2 μV_{pp} requirement. The signal magnitude spectrum of the recording is shown in Figure 5.7.

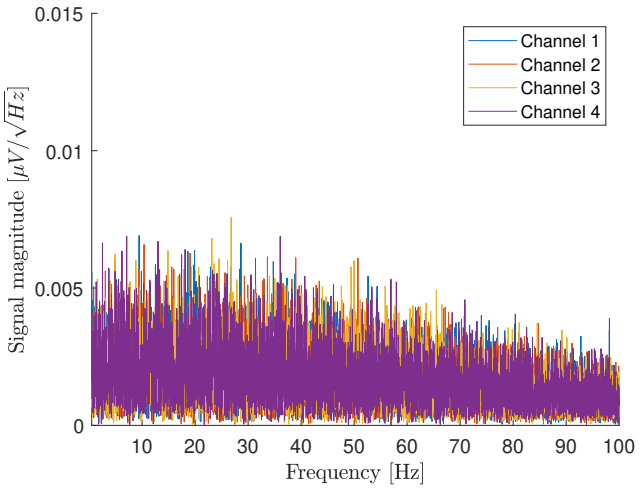

Figure 5.7: The amplitude spectrum of the final prototype with, all inputs connected to the bias electrode.

Unlike the amplitude spectrum recorded with the first prototype in Section 4.1, no peak is visible at 50 Hz. This could be because the measurements have been performed on separate occasions, at different locations, with different levels of interference. Other than the peak, the amplitude spectra look similar between the first and final prototypes.

The common-mode rejection ratio is measured at 50 Hz and 60 Hz by applying a 1 V_{RMS} sine-wave to the recording and reference electrodes, with respect to the bias electrode. The measured CMRR is shown in Table 5.1.

Table 5.1: The measured common-mode rejection ratio for the final prototype.

Frequency	**Input signal**	**Measured signal**	**CMRR**
50 Hz	1 V_{RMS}	34.8 μV_{RMS}	89.17
60 Hz	1 V_{RMS}	39.2 μV_{RMS}	88.13

The measured CMRR is higher than the measured CMRR of the first prototype, shown in Table 4.2, exceeding the minimum CMRR requirement of 80 dB.

Table 5.2 shows the idle, average, and peak power consumption of the final prototype. As expected, the power consumption is similar to that of the first prototype with one earpiece PCB connected.

Table 5.2: The average and peak power consumption of the final prototype.

Idle	**Average active**	**Peak active**
53.0 mW	63.0 mW	70.1 mW

An overview of the prototype specifications is shown in Table 5.3.

Table 5.3: Overview of the prototype specifications.

Prototype specifications	
Number of channels	4 simultaneously
Input-referred noise	0.57 μV_{pp}
Common-mode rejection	>89 dB @ 50 Hz
Input impedance at DC	1 GΩ
ADC resolution	24 bits
ADC data rate	250 SpS
Average power dissipation	63.0 mW

6

Ear-EEG experiments

6.1. Measurements setup

The final prototype is used to measure ear EEG signals. Because the in-ear electrodes are not completed at this stage of the project, the EEG signals are recorded with electrodes placed around the ears instead. This choice has been made based on the notion that the EEG signals recorded from around the ears are almost identical to those recorded from inside of the ear canal [20]. Figure 6.1 shows the locations of the electrodes during the experiment, as well as the numbering system that is used. The same dry, comb-shaped electrodes are used for the experiments as used in the experiments conducted with the first prototype.

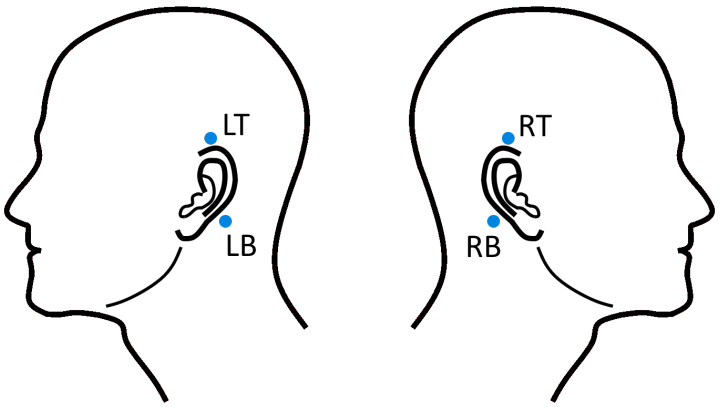

Figure 6.1: The electrode locations for the ear EEG recordings.

Each experiment is conducted 10 times with the reference electrode connected to the left earlobe, and 10 times with the reference electrode connected to the right earlobe. The bias electrode is connected to the earlobe opposite to the reference electrode. The auditory steady-state response, steady-state visual evoked potential, and alpha-band modulation paradigms are measured in these configurations. These experiments are conducted the same way as before, as described in Section 4.2.

6.2. Auditory steady-state response

The duration of the auditory steady-state response experiments is 120 s, with a modulation frequency of 40 Hz, identical to the scalp EEG experiments conducted with the first prototype. The power spectra of the experiments are shown in Figure 6.2. Table 6.1 shows the signal-to-noise ratios measured in the experiments, as well as the average per configuration. The signal-to-noise ratio is calculated by dividing the signal power at the peak by the average signal power in the frequency band between 35 Hz and 45 Hz, excluding the peak itself:

$$\text{SNR} = 10 \cdot \log_{10}(\frac{P_{peak}}{P_{35-45Hz}}). \tag{6.1}$$

The largest response has been recorded with the electrode at location LT, showing a clear peak at 40 Hz, irrespective of the location of the reference electrode. Interestingly, the response recorded with the electrode at position RT is much smaller than that recorded at electrode position LT, showing asymmetry between the ears. The measured response at electrode location RT is larger with the reference electrode connected to the right ear than with the reference electrode connected to the left ear. Electrode location RT is also located at the right ear. This shows that a two-ear setup, with the reference electrode placed at the opposite ear to the measuring electrode, does not improve the performance in this situation.

The responses recorded at locations RB and LB are of similarly small magnitude and hardly distinguishable in the power spectrum for most of the experiments.

The average signal-to-noise ratio achieved with the electrode placed at position LT is only 1.5 dB lower than the average response achieved with the best available channel in the scalp EEG experiments, performed in Section 4.2.1. This is in line with the notion that the auditory steady-state response is well detected through ear EEG, as is elaborated upon in Section 2.5.2.

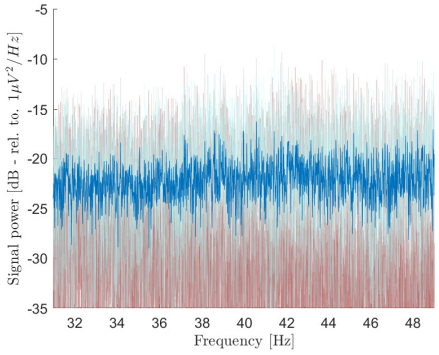

(a) Position RT - reference left

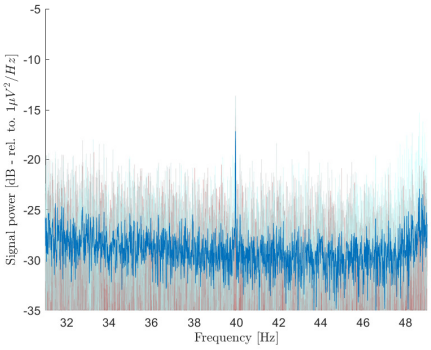

(b) Position LT - reference left

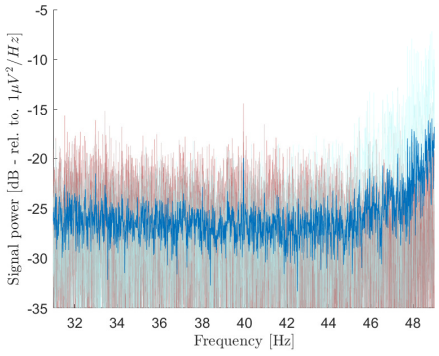

(c) Position RB - reference left

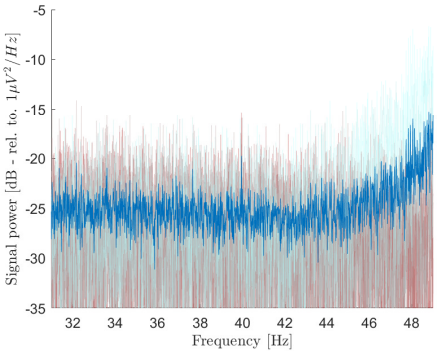

(d) Position LB - reference left

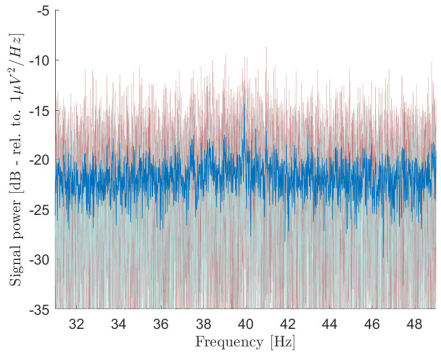

(e) Position RT - reference right

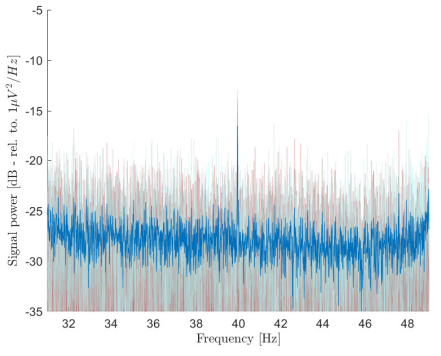

(f) Position LT - reference right

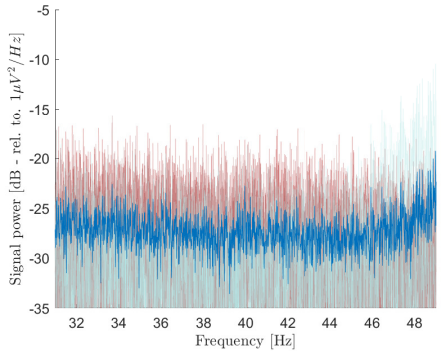

(g) Position RB - reference right

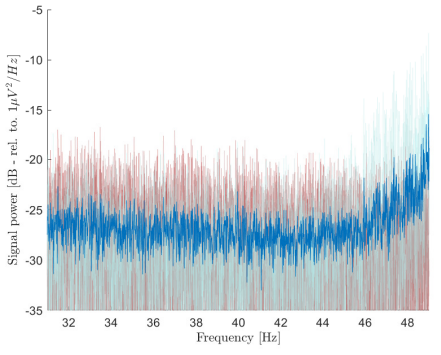

(h) Position LB - reference right

Figure 6.2: Power spectra of the ASSR experiments.

Table 6.1: Signal-to-noise ratios for each of the auditory steady-state response experiments.

	SNR (dB)							
Measuring electrode	**RT**		**LT**		**RB**		**LB**	
Reference electrode side	**L**	**R**	**L**	**R**	**L**	**R**	**L**	**R**
Experiment 1	6.32	9.33	14.93	12.94	7.70	7.34	6.98	5.18
Experiment 2	9.32	10.38	12.32	15.58	6.90	7.39	11.56	7.64
Experiment 3	7.30	8.23	10.65	12.63	11.92	7.31	9.68	8.18
Experiment 4	7.05	9.11	13.55	13.79	8.65	6.18	8.14	5.91
Experiment 5	6.60	6.35	14.30	14.94	7.72	5.90	7.60	7.34
Experiment 6	4.17	8.00	12.59	11.41	6.75	9.30	8.01	5.97
Experiment 7	3.58	14.6	14.30	15.49	6.05	7.89	6.39	5.86
Experiment 8	6.85	9.19	12.13	10.57	3.51	7.08	9.14	5.12
Experiment 9	6.17	7.69	14.33	9.70	4.11	4.74	5.01	6.38
Experiment 10	8.50	8.26	8.41	10.88	4.37	9.13	8.35	9.38
Average	**6.59**	**9.11**	**12.75**	**12.79**	**6.77**	**7.23**	**8.09**	**6.70**
Standard deviation	**1.64**	**2.10**	**1.91**	**2.02**	**2.36**	**1.32**	**1.72**	**1.32**

6.3. Steady-state visual evoked potential

An experiment duration of 60 s is used for the steady-state visual evoked potential experiments, equal to the duration used in the scalp EEG experiments performed with the first prototype. The stimulation frequency is also the same at 10 Hz. The signal-to-noise ratio is again defined as the signal power at the peak (10 Hz), divided by the average signal power in the neighbouring frequencies, ranging between 5 Hz and 15 Hz:

$$\text{SNR} = 10 \cdot \log_{10}\left(\frac{P_{peak}}{P_{5-15Hz}}\right). \tag{6.2}$$

The power spectra of the steady-state visual evoked potential experiments are shown in Figure 6.3. Table 6.2 shows the signal-to-noise ratios measured in the experiments, as well as the average per configuration. No clear peaks are visible in the power spectra at 10 Hz. This is reflected in the low signal-to-noise ratios achieved in the experiments. The achieved responses in the ear EEG experiments are much smaller than those achieved in the scalp EEG measurements performed in Section 4.2.2. In all but two of the experiments, the signal-to-noise ratio is positive, indicating that the signal power at 10 Hz is higher than the average signal power in the neighbouring frequencies. This suggests that the steady-state visual evoked potential is being recorded, although it does not result in a clear peak in the power spectra. Increasing the stimulation duration could increase the measured response, creating a more prominent peak in the power spectrum of the recordings.

The worse recording performance of the steady-state visual evoked potential from the ear recordings, compared to the scalp recordings, is in line with the expectations, as the steady-state visual evoked potential is documented to not be as well detected with ear EEG as with scalp EEG. This is elaborated upon in Section 2.5.3.

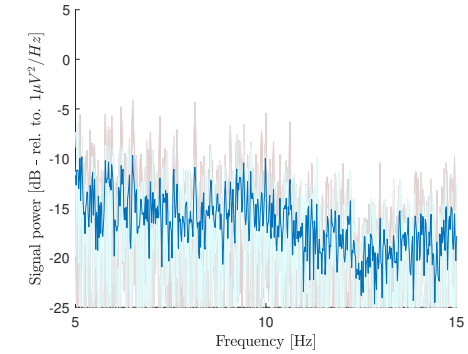

(a) Position RT - reference left

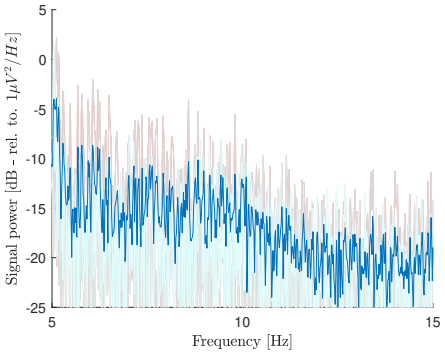

(b) Position LT - reference left

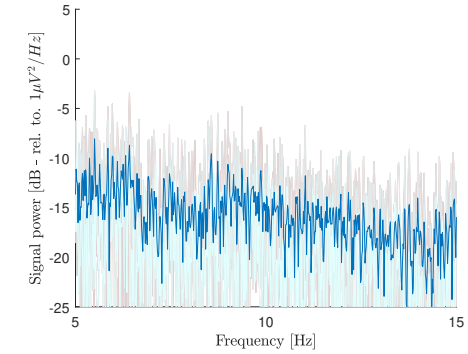

(c) Position RB - reference left

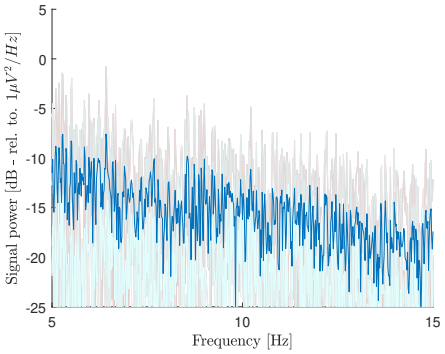

(d) Position LB - reference left

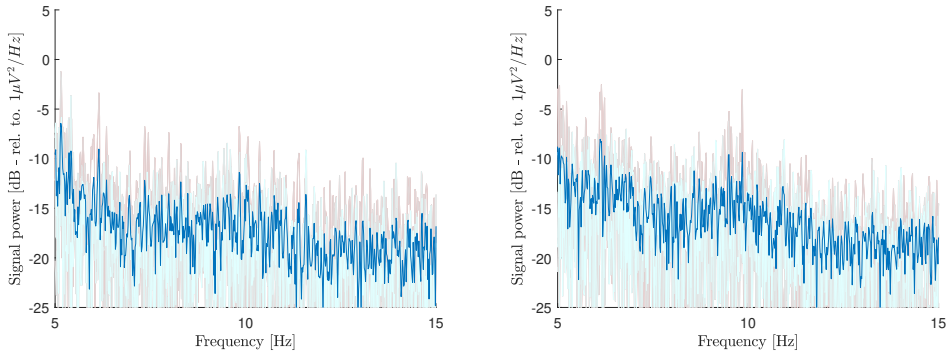

(e) Position RT - reference right

(f) Position LT - reference right

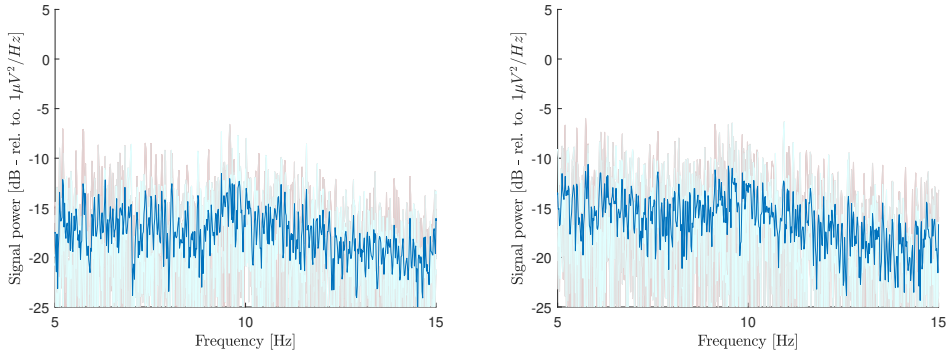

(g) Position RB - reference right

(h) Position LB - reference right

Figure 6.3: Power spectra of the SSVEP experiments.

Table 6.2: Signal-to-noise ratios for each of the steady-state visual evoked potential experiments.

	SNR (dB)							
Measuring electrode	**RT**		**LT**		**RB**		**LB**	
Reference electrode side	**L**	**R**	**L**	**R**	**L**	**R**	**L**	**R**
Experiment 1	8.59	3.85	2.76	3.06	2.95	-0.40	4.36	6.65
Experiment 2	7.01	1.09	8.09	4.58	4.76	6.06	1.93	4.62
Experiment 3	7.21	1.89	5.27	5.32	1.54	1.62	4.63	6.63
Experiment 4	6.44	7.50	7.16	2.60	4.53	9.35	6.74	7.00
Experiment 5	0.23	4.93	5.30	4.08	3.52	6.04	5.80	4.72
Experiment 6	8.59	3.85	2.76	3.06	2.95	-0.40	4.36	6.65
Experiment 7	7.01	1.09	8.09	4.58	4.76	6.06	6.74	4.62
Experiment 8	7.21	1.89	5.27	5.32	1.54	1.62	4.64	6.63
Experiment 9	6.44	7.50	7.16	2.60	4.53	9.35	6.74	7.00
Experiment 10	0.23	4.93	5.30	4.08	3.52	6.04	5.80	4.72
Average	**5.90**	**3.85**	**5.72**	**3.93**	**3.46**	**4.53**	**5.17**	**5.92**
Standard deviation	**2.92**	**2.28**	**1.83**	**0.99**	**1.16**	**3.48**	**1.43**	**1.03**

6.4. Alpha-band modulation

Figure 6.4 shows the signal power in the alpha band in each of the different configurations. Table 6.3 shows the increase in alpha-band signal power for the experiments, as well as the average increase for each configuration. An increase in the signal power has been measured between the phases in all but one of the experiments. The average increase in signal power is positive for all different electrode configurations. The highest average increase has been achieved with the electrode at location RB, with the reference electrode connected to the right ear. Electrode location RB is also located at the right ear, indicating that a two-ear setup would not be beneficial in this situation.

The second highest average power increase is measured with the electrode placed at electrode position LB, again with the reference electrode placed at the right ear. In this case, the measuring and reference electrodes are placed at opposite ears. With the reference electrode placed at the same ear, the measured average signal power increase at electrode location LB is much smaller. In this case, a two-ear setup would be beneficial. The average signal power increase is similar for the electrodes at locations RT and LT for both reference electrode positions. As the two-ear setup is not consistently the superior configuration, a one-ear setup is the most desirable option, as no connecting wires are required between earpieces.

The measured average power increase of 8.14 dB with the best available ear EEG recording channel is almost as large as the average power increase of 8.54 dB achieved with the best available scalp EEG channel in Section 4.2.3. Although the average signal power in the second phase is lower for the ear EEG experiments, the average signal power in the first phase of the experiment is also lower in the ear EEG experiments, resulting in a similar average power increase. As elaborated upon in Section 2.5.4, alpha-band modulation is typically more clearly recorded using scalp EEG than with ear EEG. This is in line with the results, although the difference between the performance between ear and scalp EEG is smaller than expected.

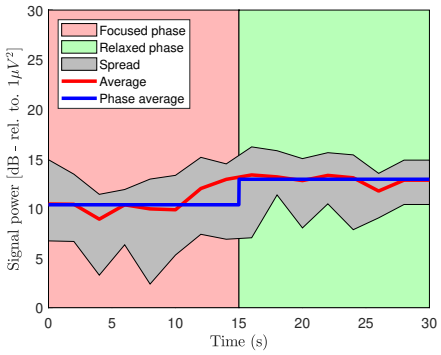

(a) Position RT - reference left

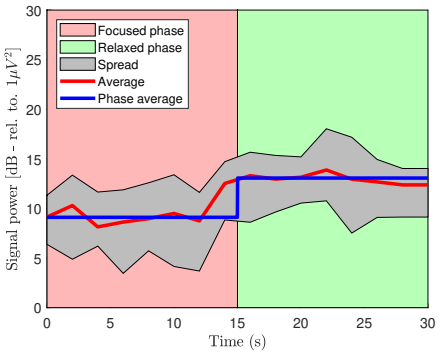

(b) Position LT - reference left

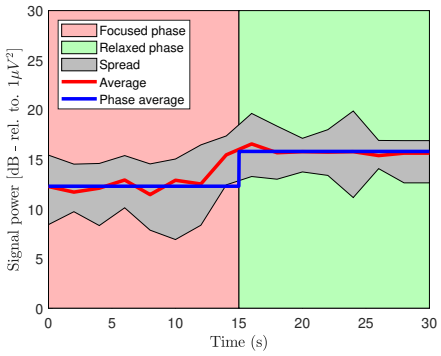

(c) Position RB - reference left

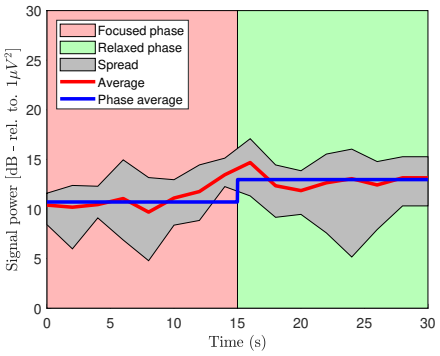

(d) Position LB - reference left

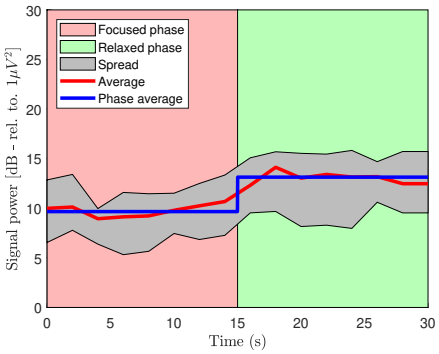

(e) Position RT - reference right

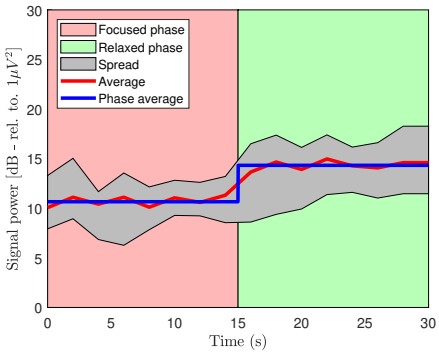

(f) Position LT - reference right

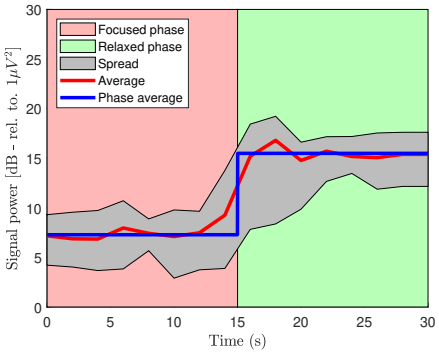

(g) Position RB - reference right

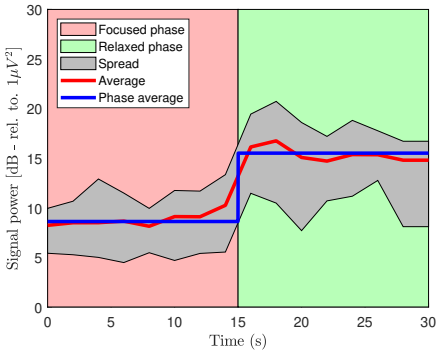

(h) Position LB - reference right

Figure 6.4: The power in the alpha band for the different configurations.

Table 6.3: The power increase in the alpha-band between the phases.

	Power increase (dB)							
Measuring electrode	**RT**		**LT**		**RB**		**LB**	
Reference electrode side	**L**	**R**	**L**	**R**	**L**	**R**	**L**	**R**
Experiment 1	1.91	1.22	0.94	2.82	2.51	7.28	3.32	6.26
Experiment 2	0.69	1.71	3.73	1.45	3.72	4.30	1.47	3.20
Experiment 3	2.33	4.32	3.67	5.00	3.35	8.20	2.02	8.04
Experiment 4	3.68	4.34	6.06	4.32	3.10	10.11	2.08	5.51
Experiment 5	2.32	3.64	4.31	4.10	3.87	8.27	2.49	6.61
Experiment 6	3.57	2.67	5.06	3.35	3.49	9.32	1.72	7.90
Experiment 7	3.54	4.06	4.23	4.44	6.87	7.47	3.06	8.07
Experiment 8	-0.11	5.52	1.90	4.56	2.32	9.20	1.27	8.53
Experiment 9	3.61	3.57	4.29	2.41	1.45	9.30	1.15	7.86
Experiment 10	5.32	3.50	5.44	3.27	4.85	7.91	3.68	5.68
Average	**2.69**	**3.46**	**3.96**	**3.57**	**3.55**	**8.14**	**2.23**	**6.77**
Standard deviation	**1.52**	**1.22**	**1.47**	**1.06**	**1.42**	**1.54**	**0.84**	**1.57**

7

Discussion and future work

7.1. Discussion

The aim of this thesis has been to design the electronics for a fully programmable, wireless in-ear EEG device, capable of onboard data processing. Based on a literature study, a list of system requirements has been created. The system components have been selected based on these requirements. The prototype consists of two main components: the Texas instruments ADS1299 analog front-end and the Nordic Semiconductor nRF5340 wireless system-on-chip. The design has been made in two iterations. In the first iteration, the aim has been to create a functional prototype, suitable for the exploration of different hardware configurations. The second iteration uses the information gathered using the first iteration to create a small form-factor prototype, suitable to be put into an earpiece.

The performance of the first prototype has been compared to the OpenBCI Cyton Biosensing Board, a larger form-factor scalp EEG recording device. The performance is compared based on the ASSR, SSVEP, and alpha-band modulation paradigms. For the ASSR and SSVEP paradigms, the performance is comparable between the devices. In the alpha-band modulation experiments, the performance of the Cyton Biosensing Board is superior to that of the prototype. The difference in the performance is mostly down to the lower signal power that is recorded in the first phase of the experiment by the Cyton Biosensing Board, compared to the prototype. A possible cause of this difference can be a worse electrode-skin connection in the experiments conducted with the prototype. As connecting each of the devices to the scalp EEG headset could not be done without taking off the headset, some variation in the electrode-skin connections could be present between the experiments. Another reason for the difference could be that the prototype is more susceptible to low-frequency interfering signals, although this is not a likely cause, as worse performance would then also be expected in the SSVEP experiments, as it concerns signals in the same frequency range.

The final prototype has been used to record ear EEG signals. As the in-ear electrodes had not yet been completed, the choice has been made to measure signals from around the ears instead. Again, the ASSR, SSVEP, and alpha-band modulation paradigms have been used to evaluate the recording performance. The ASSR and alpha-band modulation experiments showed promising results, with performance close to the scalp EEG experiments performed with the first prototype. The performance in the SSVEP experiments is significantly worse than in the scalp EEG experiments, although an increase in the signal power could be detected at the stimulation frequency in most of the experiments. The good performance for the ASSR and alpha-band modulation paradigms, and the worse performance for the SSVEP experiments, are in line with the expectations based on previous publications on in-ear EEG. The location of the measuring electrode has been found to have a large impact on the achieved performance during the experiments. An earpiece with several electrodes is therefore recommended for optimal performance. Although an increase in the signal magnitude was expected, no benefit has been found from having the reference electrode placed at the opposite ear to the measuring electrode. The two-ear setup of the first prototype does therefore not seem beneficial to the recording performance. When using in-ear electrodes, the distance between the electrodes will likely be smaller than in the experiments, in which the electrodes are placed around the ears. If for in-ear electrodes the small distance between the measuring electrodes and the reference electrode leads to a decrease in the

recording performance, placing the reference electrode somewhere close to the same ear is likely a better solution than placing it at the opposite ear. This requires shorter wires, making the setup less susceptible to interference. It also makes for a more convenient setup, not requiring a connection between the earpieces. The final prototype has been designed to fit into an earpiece, making it suitable for a one-ear setup.

The final prototype satisfies all the system requirements listed in Section 3.1. The common-mode rejection ratio of the prototype is lower than expected. This is caused by the passive low-pass filters used at the input of the analog front-end, as the capacitor shunted between the measuring and reference electrode degrades the input impedance of the prototype for higher frequencies. Because of this, part of the common-mode signal can be turned into a differential mode signal, as a result of impedance mismatch, which is then amplified by the analog-front end. The low-pass filters have been designed to have a cutoff below 8 kHz to prevent aliasing, as the maximum sampling frequency of the ADS1299 is listed as 16 SpS. A higher cutoff frequency could have been chosen. As the clock frequency that is used for the oversampled ADC is equal to 2.048 MHz, aliasing would only occur for frequencies above 1.024 MHz. A smaller capacitor could therefore be used in the passive filter, which would reduce the degradation of the input impedance for higher frequencies. This change can be made to the prototype without changing the PCB designs.

The goal of combining wireless data transmission, onboard processing, programmable hardware, and a form factor small enough to fit into an earpiece has been achieved.

7.2. Future work

This thesis is part of a larger project. Besides the electronics, this involves the design of the in-ear electrodes and the algorithms used for the data processing. At the time of writing, not all of these components have been completed. When all components are completed, they can be combined into one system. It is important to combine the components into a package that is comfortable to wear.

As the in-ear electrodes have not been finished before the end of this project, measurements from around the ears have been used to test the electronics. When the in-ear electrodes are completed, more experiments can be performed, These experiments should then be performed on a larger test group so that the results can be compared to that of other in-ear EEG devices.

During the experiments, relatively simple device firmware has been used, which transmits the entire recorded data stream using Bluetooth Low Energy. More advanced device firmware can be written, that makes use of the onboard processing capabilities of the prototype. As the system is meant as a tool to explore the possibilities of in-ear EEG, different applications can be looked into. Some interesting applications that can be explored are:

- Epileptic seizure detection
- Closed loop stimulation devices
- Brain-computer interfaces

When exploring these applications, the prototype's programmable hardware can be used to adapt the functionality of the prototype to the desired application.

If a desired in-ear EEG application has been found, a specialized prototype can be designed. By using an integrated circuit design, instead of a discrete circuit design, the prototype can be made smaller and more power efficient than the current prototype. This will come at the cost of lower flexibility of the prototype.

A

Bluetooth low energy SoCs

Table A.1: Overview of the Nordic Semiconductors nRF5 range.
Source: Adapted from [32]

	CPU	**Flash**	**RAM**	**CoreMark Score**	**Efficiency (CoreMark/mA)**
nRF5340	128 MHz Arm Cortex-M33 + 64 MHz Arm Cortex-M33	1 MB + 256 kB	512 kB + 64 kB	514	101
nRF52840	64 MHz Arm Cortex-M4 with FPU	1 MB	256 kB	212	64
nRF52833	64 MHz Arm Cortex-M4 with FPU	512 kB	128 kB	217	65.8
nRF52832	64 MHz Arm Cortex-M4 with FPU	512/256 kB	64/32 kB	215	58
nRF52820	64 MHz Arm Cortex-M4	256 kB	32 kB	144	68.6
nRF52811	64 MHz Arm Cortex-M4	192 kB	24 kB	144	65
nRF52810	64 MHz Arm Cortex-M4	192 kB	24 kB	144	65
nRF52805	64 MHz Arm Cortex-M4	192 kB	24 kB	144	65

Table A.2: Overview of the Texas Instruments CC2 range.
Source: Adapted from [39]

	CPU	Flash	RAM	CoreMark Score	Efficiency (CoreMark/mA)
CC2640R2L	48 MHz Arm Cortex-M3	128 kB + 147 kB	28 kB	142	48.5
CC2640R2F	48 MHz Arm Cortex-M3	128 kB + 147 kB	28 kB	142	48.5
CC2642R	48 MHz Arm Cortex-M4	352 kB + 256 kB	88 kB	148	43.5
CC2652x	48 MHz Arm Cortex-M4	352 kB + 256 kB	88 kB	148	43.5
CC2652x7	48 MHz Arm Cortex-M4	704 kB + 256 kB	152 kB	148	38.2

Table A.3: Overview of the NXP K32W range.
Source: Adapted from [40]

	CPU	Flash	RAM	CoreMark Score	Efficiency (CoreMark/mA)
K32W041AM	48 MHz Arm Cortex-M4	640 kB + 1 MB	152 kB	164	35
K32W041A	48 MHz Arm Cortex-M4	640 kB	152 kB	164	35
K32W061	48 MHz Arm Cortex-M4	640 kB	152 kB	164	57

Table A.4: Overview of the Silicon Labs EFR32BG22 range.
Source: Adapted from [41]

	CPU	Flash	RAM	CoreMark Score	Efficiency (CoreMark/mA)
EFR32BG22-C112F352GM32	38.4 MHz Arm Cortex-M33	352 kB	32 kB	154	105.5
EFR32BG22-C222F352GM32	76.8 MHz Arm Cortex-M33	352 kB	32 kB	309	105.9
EFR32BG22-C222F352GM40	76.8 MHz Arm Cortex-M33	352 kB	32 kB	309	105.9
EFR32BG22-C222F352GN32	76.8 MHz Arm Cortex-M33	352 kB	32 kB	309	105.9
EFR32BG22-C224F512GM32	76.8 MHz Arm Cortex-M33	512 kB	32 kB	309	105.9
EFR32BG22-C224F512GM40	76.8 MHz Arm Cortex-M33	512 kB	32 kB	309	105.9
EFR32BG22-C224F512GN32	76.8 MHz Arm Cortex-M33	512 kB	32 kB	309	105.9
EFR32BG22-C224F512IM32	76.8 MHz Arm Cortex-M33	512 kB	32 kB	309	105.9
EFR32BG22-C224F512IM40	76.8 MHz Arm Cortex-M33	512 kB	32 kB	309	105.9

B

Component diagrams

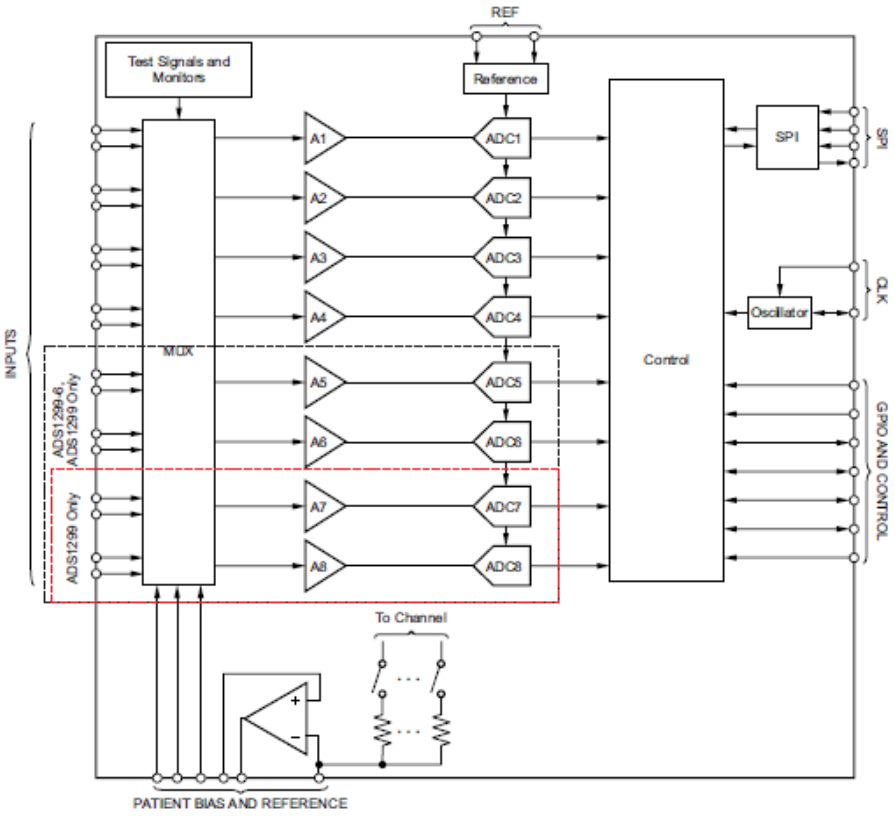

Figure B.1: Block diagram of the ADS1299. Source: Adapted from [28]

C

PCB schematics

C.1. First prototype

C.1.1. Microcontroller PCB

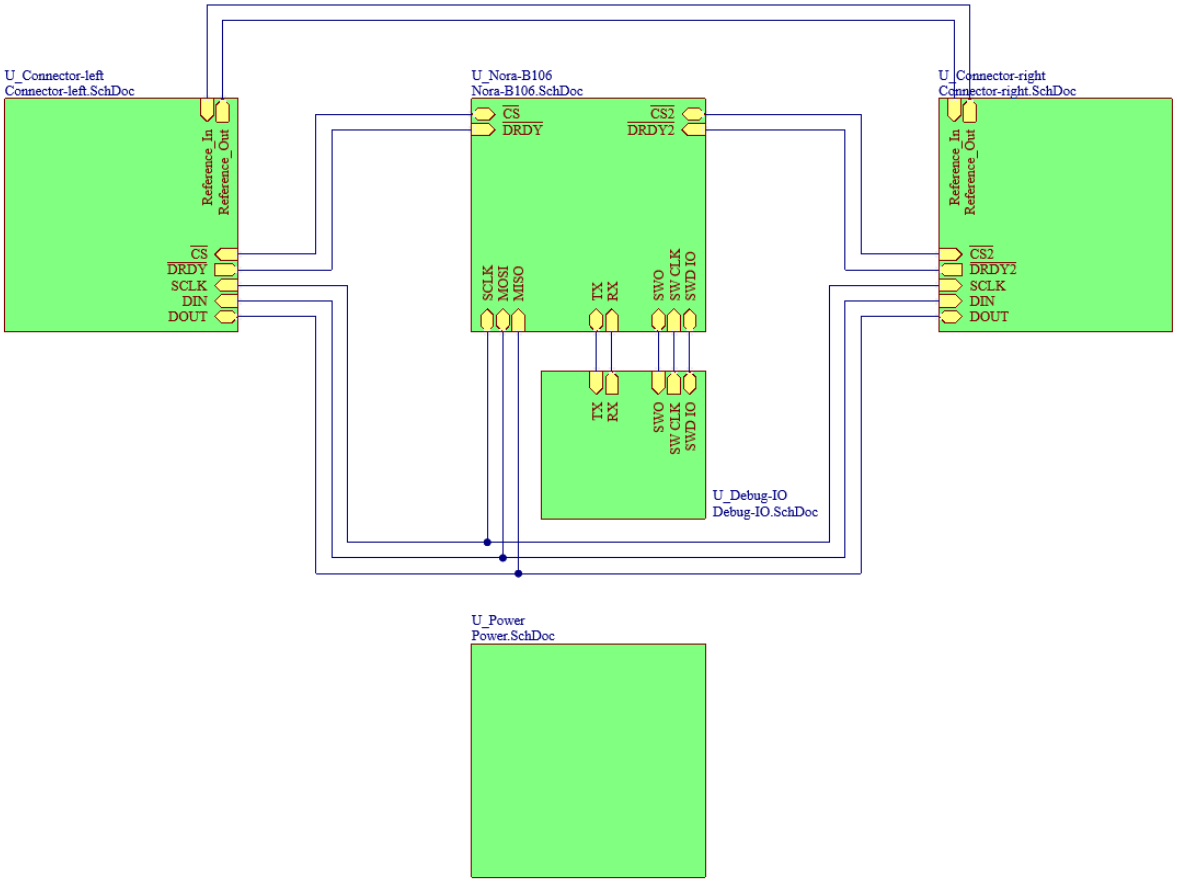

Figure C.1: Schematic overview of the microcontroller PCB.

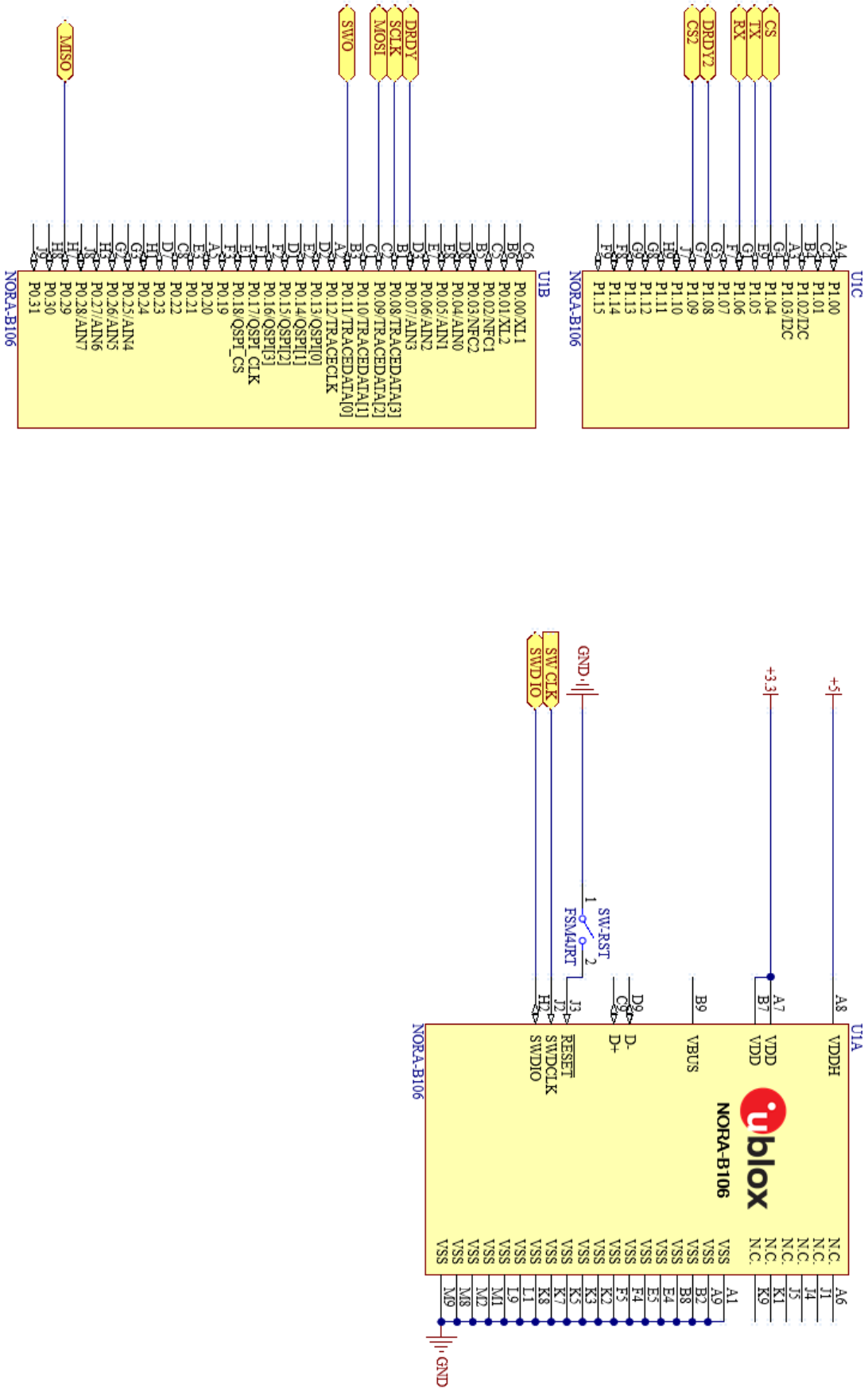

Figure C.2: Schematic of the micro controller module.

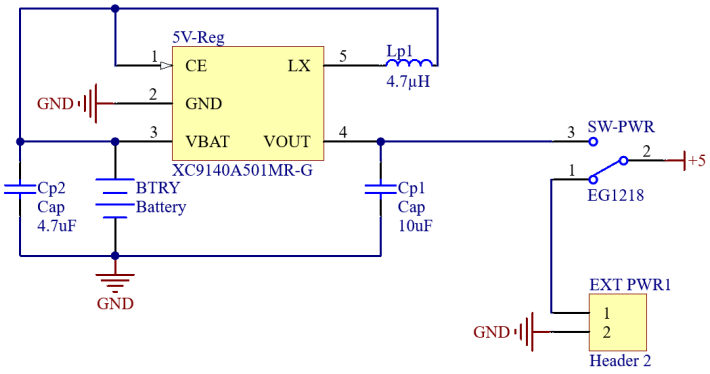

Figure C.3: Schematic of power system module.

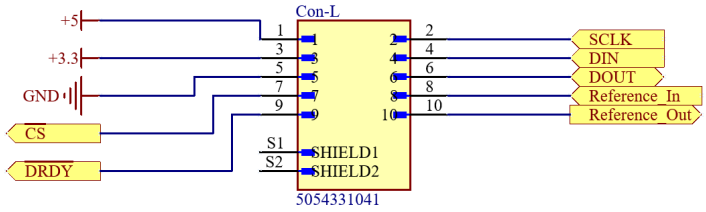

Figure C.4: Schematic of the left side connector module.

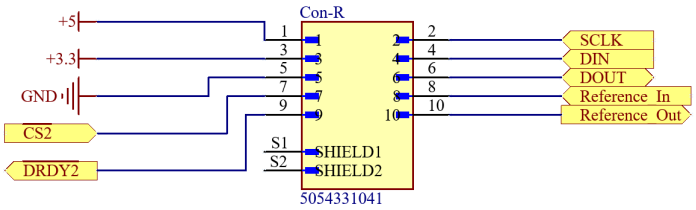

Figure C.5: Schematic of the right side connector module.

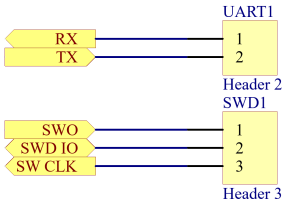

Figure C.6: Schematic of the debug interface module.

C.1.2. Earpiece PCB

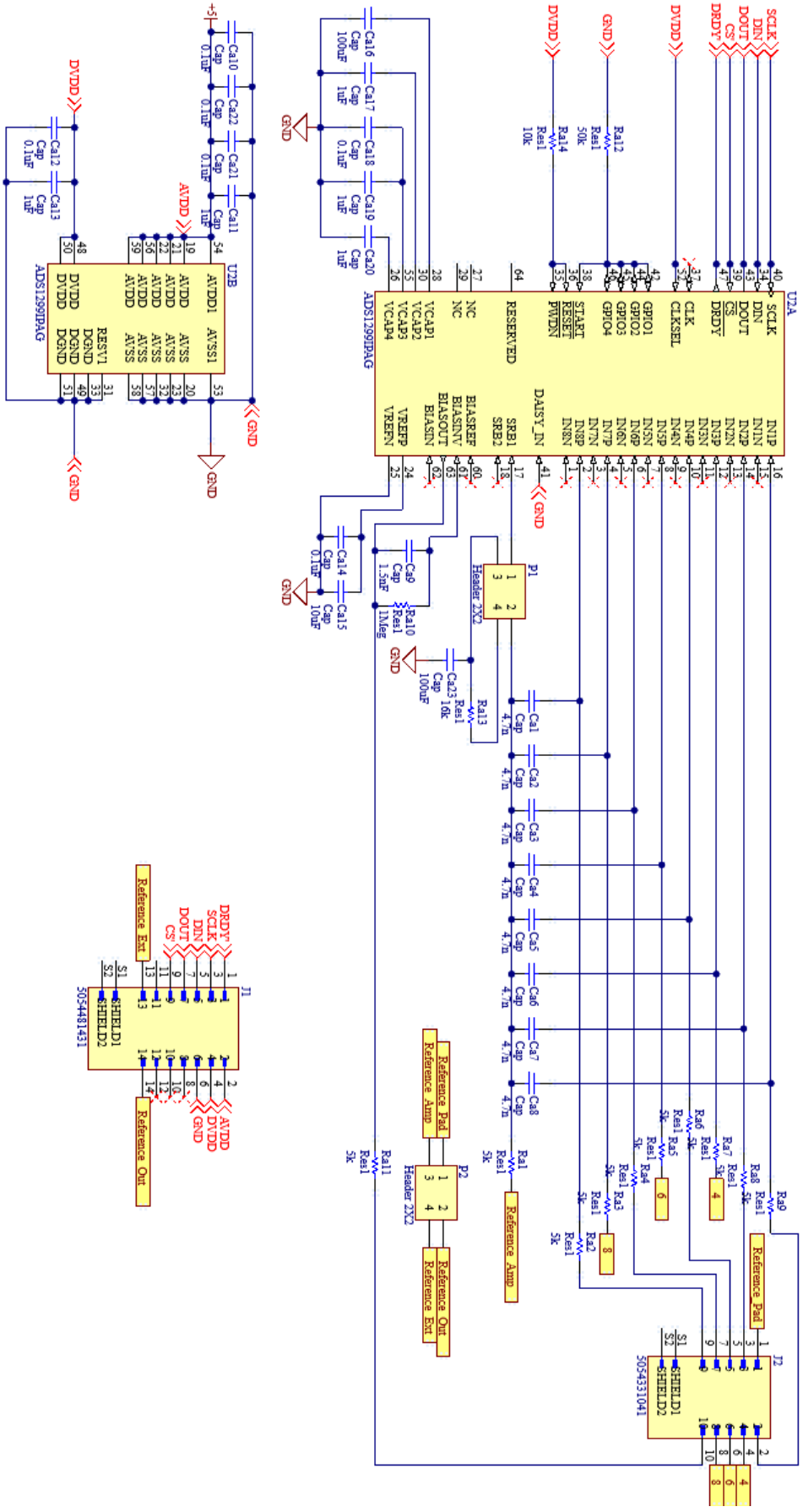

Figure C.7: Schematic of the analog front-end PCB.

C.2. Final prototype

C.3. Microcontroller PCB

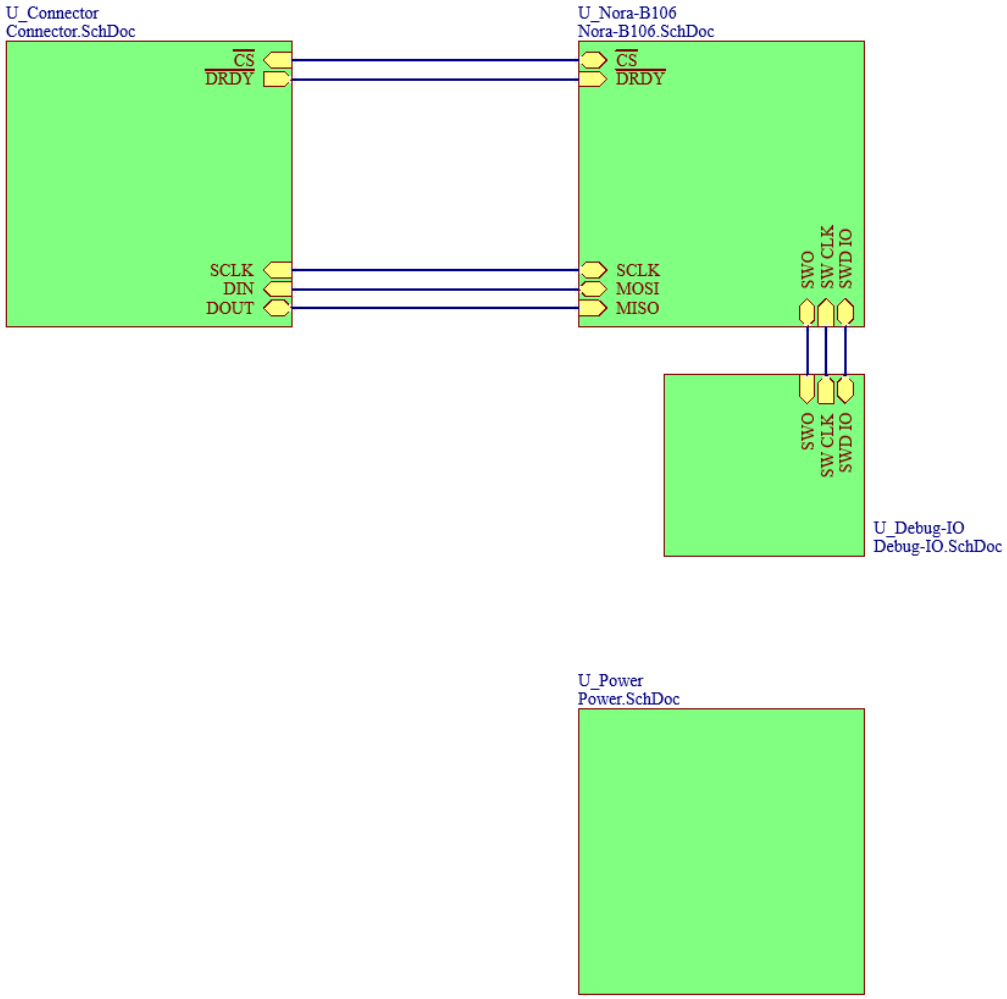

Figure C.8: Schematic overview of the microcontroller PCB.

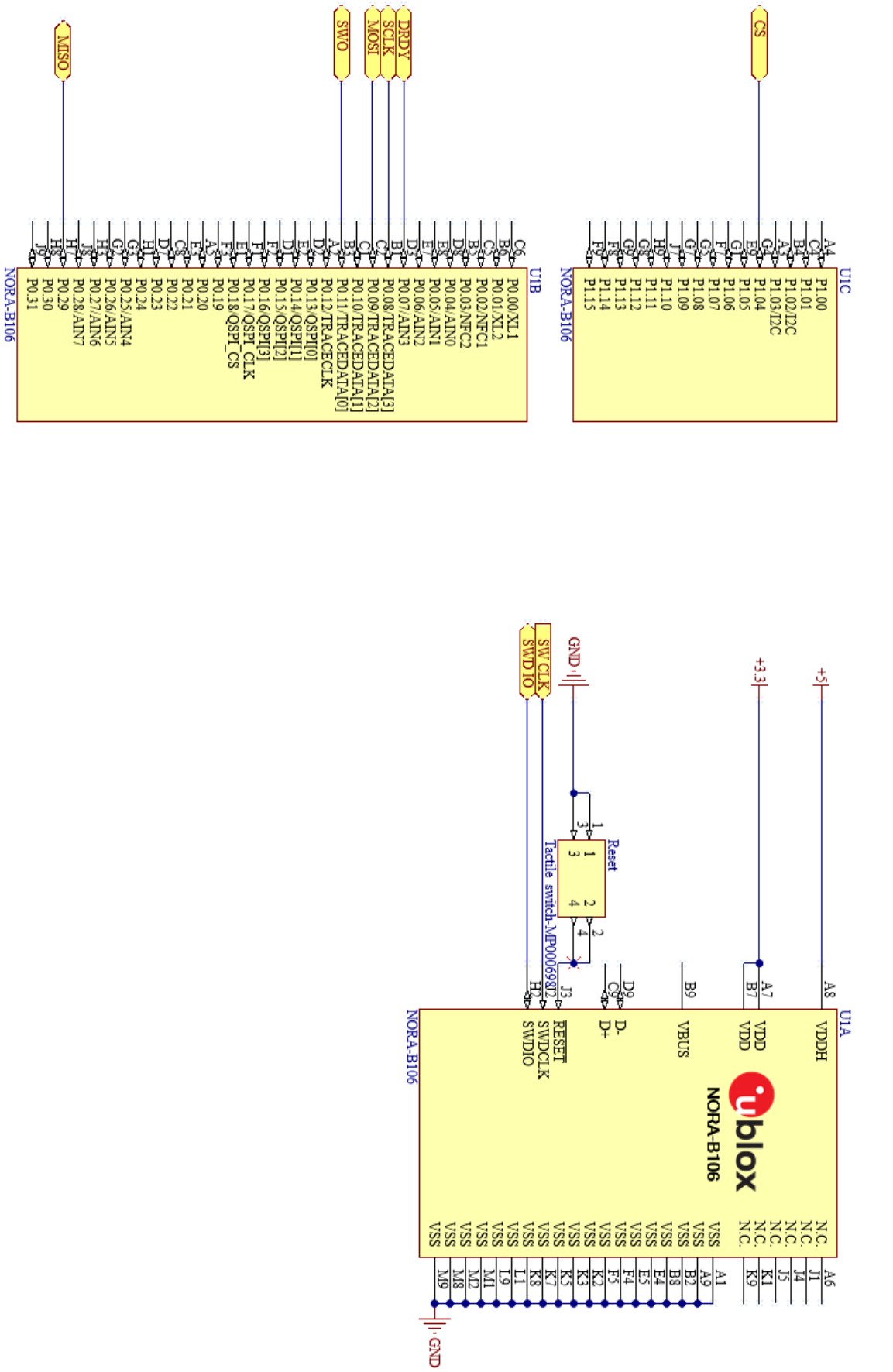

Figure C.9: Schematic of the micro controller module.

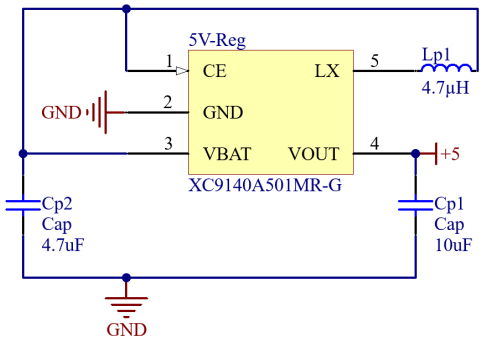

Figure C.10: Schematic of power system module.

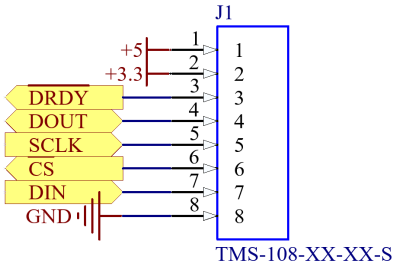

Figure C.11: Schematic of the left side connector module.

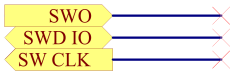

Figure C.12: Schematic of the debug interface module.

C.3.1. Analog front-end PCB

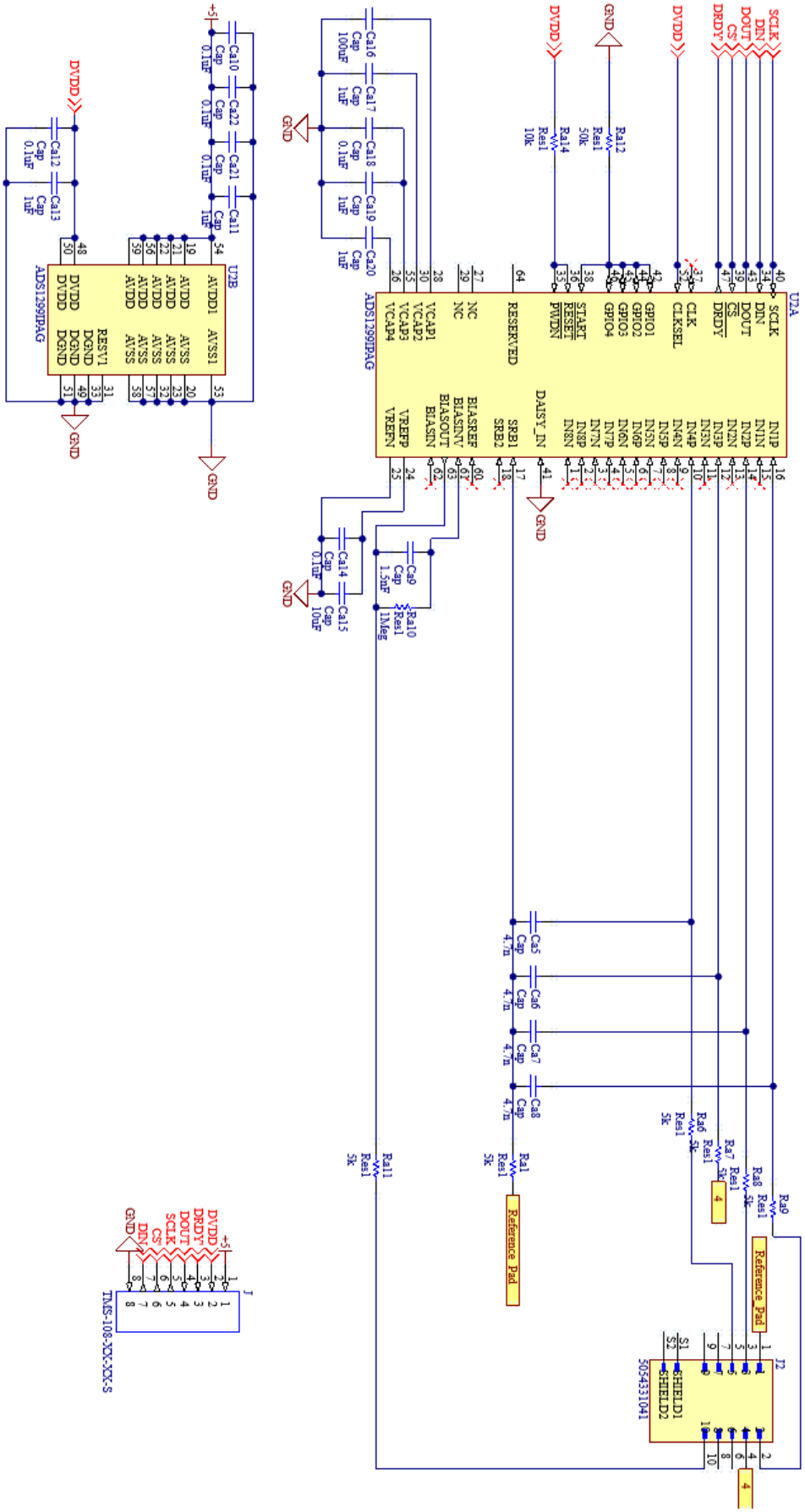

Figure C.13: Schematic of the analog front-end PCB.

D

Filtered reference

In-ear EEG recording comes with limitations for the positioning of electrodes, as all electrodes are placed inside the ear. Because of this, the distance between electrodes can not be very large. This can result in similar signals being recorded at the measuring and reference electrodes, resulting in a small magnitude measured signal after differential amplification. This issue is visualised in Figure D.1.

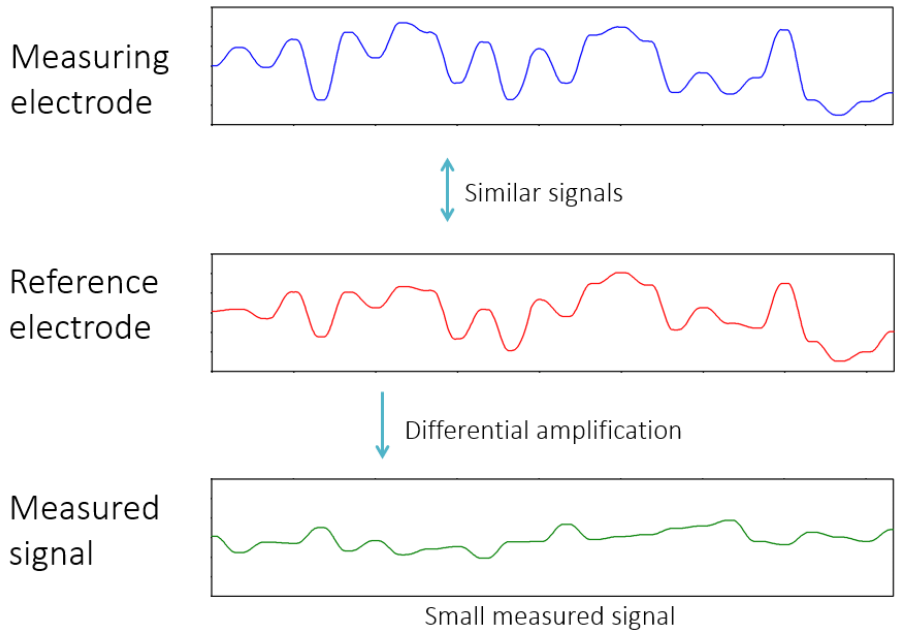

Figure D.1: Similar signals are present at the reference and measuring electrode, resulting in a small magnitude measured signal.

To get around this issue, a two-ear setup has been proposed. By using a reference electrode placed at the opposite ear, a larger difference is expected between the signals seen at the measuring and reference electrodes, in theory creating a measured signal of larger magnitude, as shown in Figure D.2.

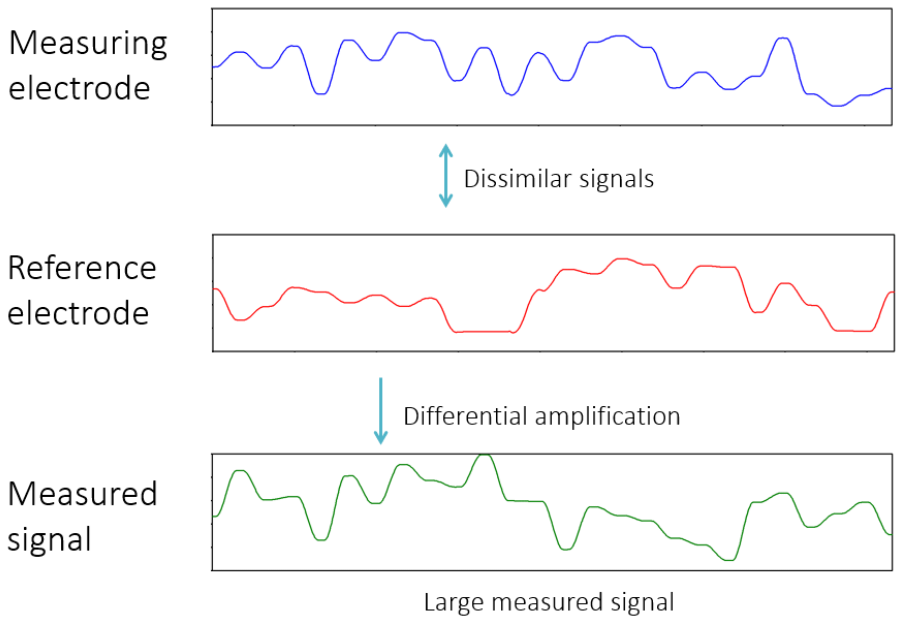

Figure D.2: Dissimilar signals are present at the reference and measuring electrode, resulting in a large magnitude measured signal.

Another method of resolving the same issue is proposed: By applying a low-pass filter to the signal seen at the reference electrode, all frequencies above 0.1 Hz are removed from the spectrum, leaving a near DC signal as a reference. As no EEG signals are present in this reference signal, the measured signal will be equal to the EEG signal seen at the measuring electrode. This approach could improve the measurement performance when referencing to the same ear, as the problem of similar signals being seen at the reference and measuring electrodes is mitigated. Figure D.3 shows this concept.

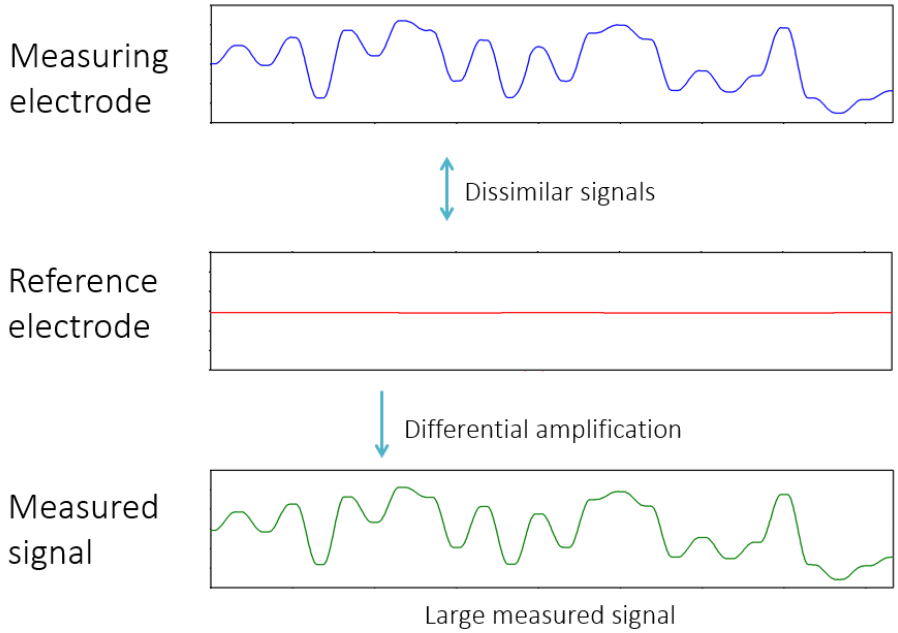

Figure D.3: The reference electrode is filtered, resulting in a large magnitude measured signal.

When testing the concept in practice, the results are not as expected beforehand. In the proposed concept, different locations on the scalp are treated as separate sources that can separately be filtered. In reality, this

is not the case. Applying the filter results in all EEG signals being filtered out, resulting in a recorded near-DC signal. This can be explained by the entire scalp being grounded for frequencies above 0.1 Hz.

E

ADS1299 commands

Table E.1: Command definitions for the ADS1299
Source: Adapted from [28]

COMMANDS	DESCRIPTION	FIRST BYTE	SECOND BYTE
System Commands			
WAKEUP	Wake-up from standby mode	0000 0010 (02h)	
STANDBY	Enter standby mode	0000 0100 (04h)	
RESET	Reset the device	0000 0110 (06h)	
START	Start and restart (synchronize) conversions	0000 1000 (08h)	
STOP	Stop conversion	0000 1010 (0Ah)	
Data Read Commands			
RDATAC	Enable Read Data Continuous mode. This mode is the default mode at power-up.	0001 0000 (10h)	
SDATAC	Stop Read Data Continuously mode	0001 0001 (11h)	
RDATA	Read data by command; supports multiple read back.	0001 0010 (12h)	
Register Read Commands			
RREG	Read n nnnn registers starting at address r rrrr	001r rrrr (2xh) [1]	000n nnnn [1]
WREG	Write n nnnn registers starting at address r rrrr	010r rrrr (4xh) [1]	000n nnnn [1]

[1] n nnnn = number of registers to be read or written – 1. For example, to read or write three registers, set n nnnn = 0 (0010).
r rrrr = starting register address for read or write commands.

F

Prototype V1.0 - Jumper positions

The different jumper positions that are available are shown in Figure F.1. Table F.1 lists the configurations corresponding to the jumper positions.

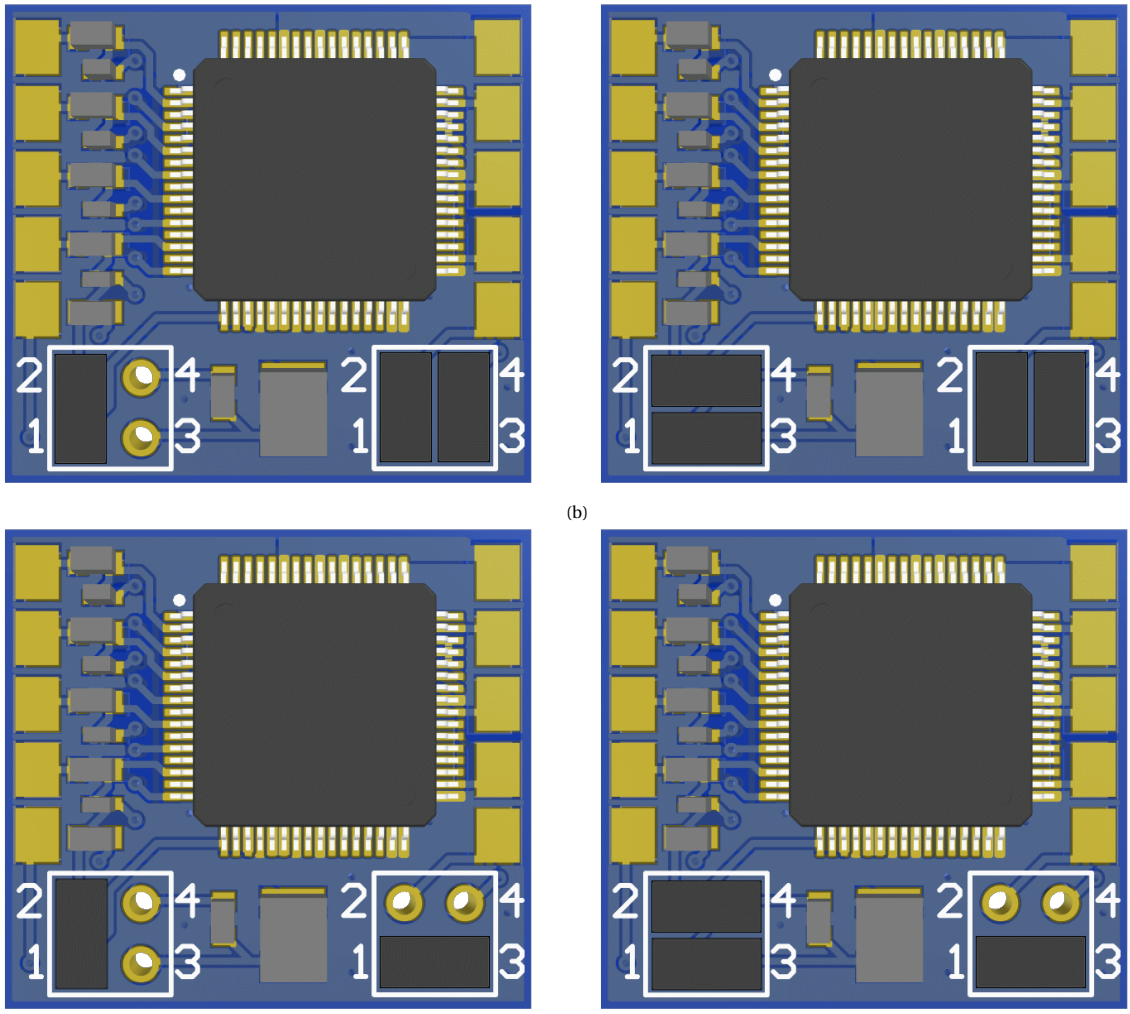

(a) (b)

(c) (d)

Figure F.1: The different jumper positions for the first prototype.

Table F.1: The configurations corresponding to the jumper positions.

Configuration	**Reference electrode**	**Filtered electrode**
a	External	No
b	External	Yes
c	Local	No
d	Local	Yes

G

Software

G.1. Device firmware

The device firmware is written in C, using the nRF Connect SDK kit provided by Nordic Semiconductor. The SDK provides many example projects that can be used as a basis for the firmware for the devices in the nRF range of microcontrollers. The firmware that is used on the prototype is based on an example project that enables the Bluetooth low-energy functionality of the device. The project is altered to allow for communication to the ADS1299 analog front-ends using the serial peripheral interface (SPI). The data that is received via the SPI communication is placed in a buffer to be transmitted using Bluetooth low-energy. A Bluetooth low-energy service is created to transmit the data. Other devices can receive the recorded data by subscribing to the service. A second service is created that is used to receive data from other devices. This service is used to communicate with the recording software. Based on the data received in the service, the bias electrode and test signal of the ADS1299 can be configured. This is done by sending commands to the ADS1299 using the SPI connection. A complete overview of the available commands is shown in Appendix E.1. The service can also be used to start and set the duration of a recording.

G.2. Recording software

The recording software has been written using Python. Figure G.1 shows an image of the user interface.

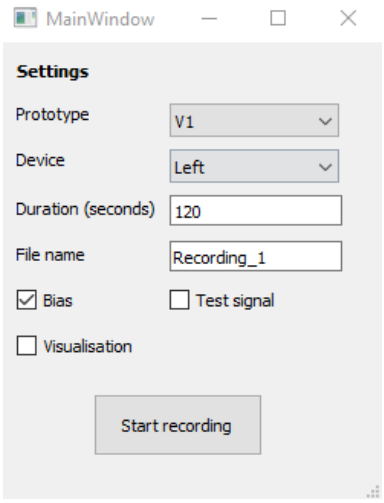

Figure G.1: The user interface of the recording application.

The 'prototype' field can be used to select either the first or second prototype iteration. The 'device' dropdown box can then be used to select either the left or right earpiece for recording. The duration of the recording can be entered in the 'duration' field and the file name can be entered in the 'File name' field. The bias electrode

can be enabled by checking the 'Bias' box. The recording is started by pressing the 'Start recording' button. The 'Test signal' checkbox can be used to activate the test signal on the ADS1299 analog front-end.

The recorded data is stored in a .txt file, compatible with the OpenBCI GUI software [42].

Live visualisation of the recording can be activated by checking the 'Visualisation' box.

G.3. Stimulation software

G.3.1. Auditory steady-state response

The auditory steady-state response stimulation software generates an amplitude-modulated audio signal. The application has been designed using the MATLAB App Designer. Figure G.2 shows the user interface of the application.

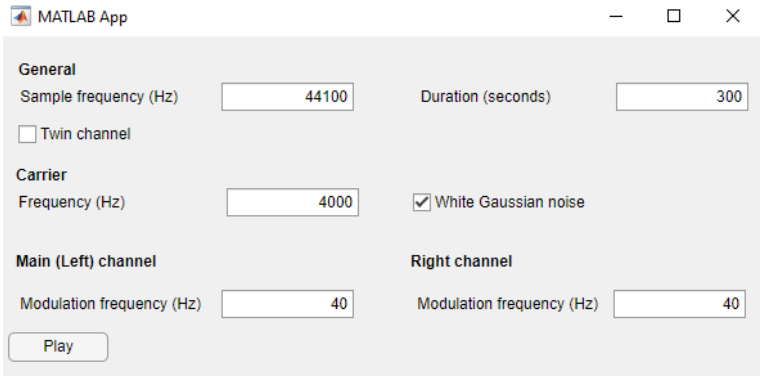

Figure G.2: The user interface of the auditory steady-state response stimulation software.

In the 'General' section, the sample rate and stimulation duration can be set using the two input fields. The twin channel checkbox can be used to enable different stimulation settings for the left and right audio channels. This can be used in experiments where the subject focuses on one of the two audio channels, to make it more dominant in the EEG recording than the other channel. In the 'Carrier' section, the frequency of the carrier wave can be chosen. The white Gaussian noise checkbox can be checked to use a white Gaussian noise signal instead of a sine wave as the carrier signal. Doing so overrides the carrier frequency field. In the 'Main (Left) channel' section, the frequency of the amplitude modulation can be set using the input field. When the twin channel functionality is enabled, the field can be used to set the modulation frequency for the left channel. The 'Right channel' section can then be used to set the modulation frequency for the right channel. The 'Right channel' section is not used when the twin channel functionality is not enabled.

G.3.2. Steady-state visual evoked potential

The steady-state visual evoked potential stimulation application has been designed using Python. The user interface of the application is shown in Figure G.3. The frequency and duration of the stimulation can be set using the respective input fields and stimulation is started using the start button. When stimulation is started, the black panel starts toggling between black and red at the selected frequency. Stimulation automatically stops after the entered duration.

G.3.3. Alpha-band modulation

The alpha-band modulation stimulation software generates simple math problems to be solved by the subject. This ensures the subject is in a focused state. The subject is then asked to close their eyes and relax, which should cause an increase in the amount of alpha waves present in the EEG recording. The user interface of the application is shown in Figure G.4.

Figure G.3: The user interface of the auditory steady-state response stimulation software.

Figure G.4: The user interface of the alpha-band modulation stimulation software.

The session duration can be set using the left input field. During the first half of the session duration, math problems are shown to the subject. A new problem is generated every 2 seconds. After half of the session duration has passed, the subject is asked to close their eyes and relax for the remainder of the session. When the session has been completed, a tone is played, signalling to the subject they can open their eyes again. The number of successive sessions can be set using the right input field. The total duration of the experiment will be equal to the session duration times the number of sessions. Figure G.5 shows the application in the focusing and relaxing phases.

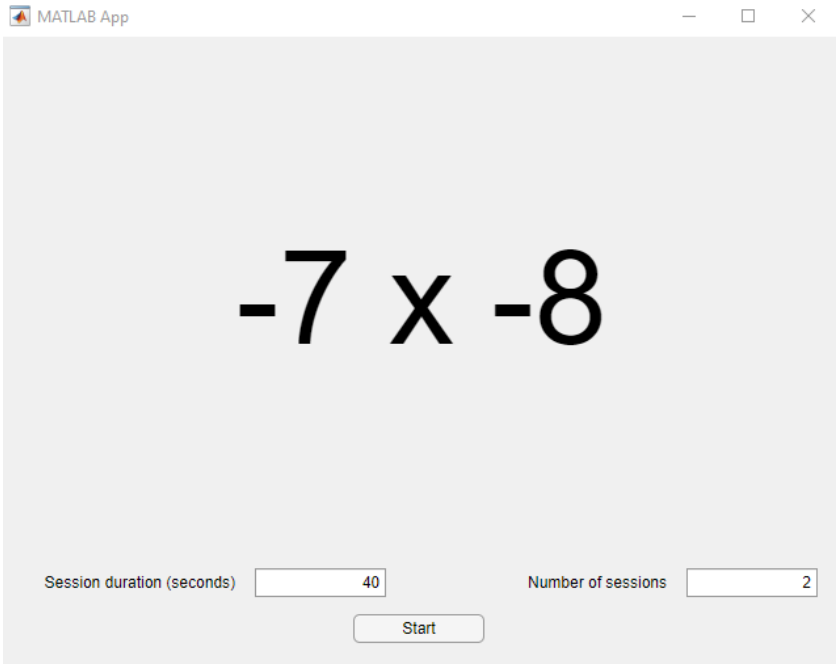

(a) Focusing phase

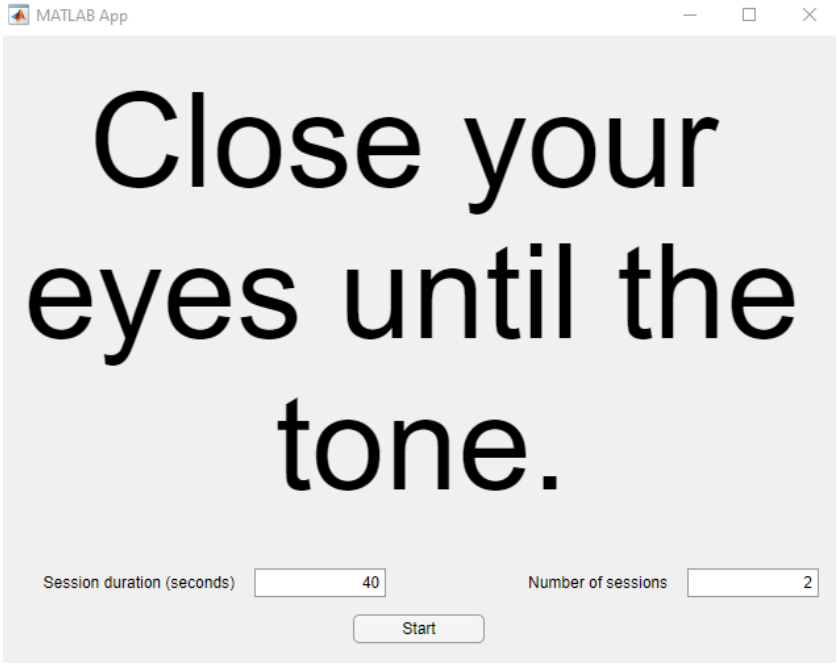

(b) Relaxing phase

Figure G.5: The alpha-band modulation application in the focusing and relaxing phases.

Bibliography

[1] Baburov, File:eeg registration.jpg, Aug. 2009. [Online]. Available: https://commons.wikimedia.org/wiki/Category:Electroencephalography.

[2] R. Kaveh, J. Doong, A. Zhou, et al., "Wireless user-generic ear eeg," IEEE Transactions on Biomedical Circuits and Systems, vol. 14, no. 4, pp. 727–737, 2020.

[3] G. Sintotskiy and H. Hinrichs, "In-ear-eeg–a portable platform for home monitoring," Journal of medical engineering & technology, vol. 44, no. 1, pp. 26–37, 2020.

[4] J. Lee, K.-R. Lee, U. Ha, et al., "A 0.8-v 82.9-µw in-ear bci controller ic with 8.8 pef eeg instrumentation amplifier and wireless ban transceiver," IEEE Journal of Solid-State Circuits, vol. 54, no. 4, pp. 1185–1195, 2019.

[5] P. Burgar, Patricija burgar, Nov. 2021. [Online]. Available: http://bioelectronics.tudelft.nl/Education/bio.php?id=1366.

[6] M. Treffers, Michael treffers, Oct. 2021. [Online]. Available: http://bioelectronics.tudelft.nl/Education/bio.php?id=1368.

[7] K. Aboalayon, M. Faezipour, W. Almuhammadi, and S. Moslehpour, "Sleep stage classification using eeg signal analysis: A comprehensive survey and new investigation," Entropy, vol. 18, Aug. 2016. DOI: 10.3390/e18090272.

[8] P. A. Abhang, B. W. Gawali, and S. C. Mehrotra, Introduction to EEG-and speech-based emotion recognition. Academic Press, 2016.

[9] M. Teplan et al., "Fundamentals of eeg measurement," Measurement science review, vol. 2, no. 2, pp. 1–11, 2002.

[10] A. Searle and L. Kirkup, "A direct comparison of wet, dry and insulating bioelectric recording electrodes," Physiological measurement, vol. 21, no. 2, p. 271, 2000.

[11] Y. Sun, N. Ye, and F. Pan, "A novel design of eeg signal amplifier," in 2012 24th Chinese Control and Decision Conference (CCDC), IEEE, 2012, pp. 3369–3372.

[12] C. Weustink, Impedance offset. [Online]. Available: https://docs.google.com/spreadsheets/d/1rs8zHTYZNo1DDZbQPxU9vgnFrAJ_ZI6V/edit?usp=sharing&ouid=118154414922856526252&rtpof=true&sd=true.

[13] G. Deuschl and A. Eisen, Recommendations for the practice of clinical neurophysiology: guidelines of the International Federation of Clinical Neurophysiology. Elsevier, 1999.

[14] B. Li, T. Cheng, and Z. Guo, "A review of eeg acquisition, processing and application," in Journal of Physics: Conference Series, IOP Publishing, vol. 1907, 2021, p. 012 045.

[15] J. Bronzino, "The biomedical engineering handbook," 1995.

[16] W. Kester and J. Bryant, "Section 3-2 - adc architectures," in Data Conversion Handbook, W. Kester, Ed., Burlington: Newnes, 2005, pp. 175–230, ISBN: 978-0-7506-7841-4. DOI: https://doi.org/10.1016/B978-075067841-4/50016-6. [Online]. Available: https://www.sciencedirect.com/science/article/pii/B9780750678414500166.

[17] R. Sarpeshkar, "Ultra low power bioelectronics: Fundamentals, biomedical applications, and bio-inspired systems," 2010.

[18] N. S. Dias, J. P. Carmo, P. M. Mendes, and J. H. Correia, "Wireless instrumentation system based on dry electrodes for acquiring eeg signals," Medical engineering & physics, vol. 34, no. 7, pp. 972–981, 2012.

[19] M. Ghamari, H. Arora, R. S. Sherratt, and W. Harwin, "Comparison of low-power wireless communication technologies for wearable health-monitoring applications," in 2015 International Conference on Computer, Communications, and Control Technology (I4CT), 2015, pp. 1–6. DOI: 10.1109/I4CT.2015.7219525.

[20] K. B. Mikkelsen, S. L. Kappel, D. P. Mandic, and P. Kidmose, "Eeg recorded from the ear: Characterizing the ear-eeg method," Frontiers in neuroscience, vol. 9, p. 438, 2015.

[21] S. L. Kappel, M. L. Rank, H. O. Toft, M. Andersen, and P. Kidmose, "Dry-contact electrode ear-eeg," IEEE Transactions on Biomedical Engineering, vol. 66, no. 1, pp. 150–158, 2018.

[22] T. W. Picton, M. S. John, A. Dimitrijevic, and D. Purcell, "Human auditory steady-state responses: Respuestas auditivas de estado estable en humanos," International journal of audiology, vol. 42, no. 4, pp. 177–219, 2003.
[23] S. E. P. Nomenclature, "American electroencephalographic society guidelines for," Journal of clinical Neurophysiology, vol. 8, no. 2, pp. 200–2, 1991.
[24] P. Kidmose, D. Looney, M. Ungstrup, M. L. Rank, and D. P. Mandic, "A study of evoked potentials from ear-eeg," IEEE Transactions on Biomedical Engineering, vol. 60, no. 10, pp. 2824–2830, 2013.
[25] V. Goverdovsky, D. Looney, P. Kidmose, and D. P. Mandic, "In-ear eeg from viscoelastic generic earpieces: Robust and unobtrusive 24/7 monitoring," IEEE Sensors Journal, vol. 16, no. 1, pp. 271–277, 2015.
[26] A. Zhou, S. R. Santacruz, B. C. Johnson, et al., "Wand: A 128-channel, closed-loop, wireless artifact-free neuromodulation device," arXiv: Neurons and Cognition, 2017.
[27] B. C. Johnson, S. Gambini, I. Izyumin, et al., "An implantable 700µw 64-channel neuromodulation ic for simultaneous recording and stimulation with rapid artifact recovery," 2017 Symposium on VLSI Circuits, pp. C48–C49, 2017.
[28] Low-noise, 8-channel, 24-bit analog-to-digital converter for biopotential measurements, ADS1299, Rev. C, Texas Instruments, Jan. 2017.
[29] Low power, five electrode electrocardiogram (ecg) analog front end, ADAS1000, Rev. C, Analog Devices, 2018.
[30] Diagnostic-quality acquisition system for bio-electric sensors and bio-impedance measurements, HM301D, Rev. 5.1, ST Microelectronics, Aug. 2018.
[31] W. Shi, J. Zhang, Z. Zhang, L. Hu, and Y. Su, "An introduction and review on innovative silicon implementations of implantable/scalp eeg chips for data acquisition, seizure/behavior detection, and brain stimulation," Brain Science Advances, vol. 6, no. 3, pp. 242–254, 2020.
[32] Bluetooth low energy. [Online]. Available: https://www.nordicsemi.com/Products/Bluetooth-Low-Energy.
[33] Xc9140 series, XC9140, Rev. 9a, Torex, 2012.
[34] Nora-b1 series, NORA-B1, R09, UBlox, 2022.
[35] Nrf5340 dk - development kit for the nrf5340, a dual-core bluetooth 5.2 soc supporting bluetooth low energy, bluetooth mesh, nfc, thread and zigbee. [Online]. Available: https://www.nordicsemi.com/Products/Development-hardware/nrf5340-dk.
[36] Cyton board: Openbci documentation, Jul. 2021. [Online]. Available: https://docs.openbci.com/Cyton/CytonLanding/.
[37] Ultracortex mark iv: Openbci documentation, Dec. 2021. [Online]. Available: https://docs.openbci.com/AddOns/Headwear/MarkIV/.
[38] Emmerich er 14250. [Online]. Available: https://www.conrad.nl/nl/p/emmerich-er-14250-speciale-batterij-1-2-aa-lithium-3-6-v-1200-mah-1-stuk-s-651240.html.
[39] Bluetooth® products. [Online]. Available: https://www.ti.com/wireless-connectivity/bluetooth/overview.html.
[40] Bluetooth smart/bluetooth low energy. [Online]. Available: https://www.nxp.com/products/wireless/bluetooth-low-energy:bluetooth-low-energy-ble.
[41] Efr32bg22 series 2 bluetooth low energy (soc) - silicon labs, Feb. 2021. [Online]. Available: https://www.silabs.com/wireless/bluetooth/efr32bg22-series-2-socs#.
[42] The openbci gui: Openbci documentation, Jul. 2022. [Online]. Available: https://docs.openbci.com/Software/OpenBCISoftware/GUIDocs/.